

Tunable $t - t' - U$ Hubbard models in twisted square homobilayers

P. Myles Eugenio,^{1,2,*} Zhu-Xi Luo,^{2,†} Ashvin Vishwanath,^{2,‡} and Pavel A. Volkov^{1,2,§}

¹*Department of Physics, University of Connecticut, Storrs, Connecticut 06269, USA*

²*Department of Physics, Harvard University, Cambridge, Massachusetts 02138, USA*

Square lattice Hubbard models with tunable hopping ratio t'/t are highly promising for realizing a variety of quantum phases and for shedding light on key puzzles in correlated quantum materials, including higher-temperature superconductivity. We show that twisted square lattice homo-bilayers generically offer such tunability when the flat bands originate from the corner of the Brillouin zone. We reveal an emergent symmetry at low twist-angles, absent in single layers, that necessitates the vanishing of nearest neighbor hopping ($t = 0$). This symmetry can be lifted by an inter-layer displacement field or by an in-plane magnetic field, introducing tunable t and anisotropy, allowing access to a wide range of t'/t ratios for correlated electrons on a moiré square lattice.

The discovery of two-dimensional Van der Waals materials [1–3] has recently led to the realization of a number of exotic states of matter in twisted multilayers, which feature moiré lattices [4]. These materials have been shown to have the capability to simulate important quantum Hamiltonians such as the Hubbard model [5, 6] or Ising, XY and Heisenberg models [7], with parameters tunable in-situ by, e.g. gating [5, 8].

While the great majority of the current moiré materials are built from hexagonal layers[9], there is significant interest in achieving highly tunable *square lattice* platforms. The square lattice Hubbard model is widely believed to capture the essential physics of the cuprates including high- T_c superconductivity[10–17], and has motivated the development of other square lattice based materials. Such a program has recently led to successful fabrication of new unconventional superconductors [18–20] and motivated experiments on tunable cold-atom fermionic Hubbard models [21]. However, accessing low temperature physics in the latter remains an ongoing challenge, emphasizing the significant advantage of moiré platforms that combine tunability with elevated electronic energy scales. Here we outline a strategy towards achieving a tunable square lattice Hubbard model that relies on a novel aspect of moiré materials, the emergence of new symmetries in the limit of low twist angles.

Previously, extensions beyond hexagonal symmetry were considered for different 2D Bravais lattices, including the square lattice [22], where in addition to crystalline symmetry, the Brillouin zone position of the band top/bottom plays a key role. Twisted square lattices are being explored in the contexts of twisted bilayers of staggered or uniform flux states [23, 24], states with quadratic band touching [25], twisted cuprates [26–31] and FeSe [32]. They have also been recently implemented in a number of analogue systems, such as cold atoms [33–35], optical [36–38] and acoustic [39] metamaterials.

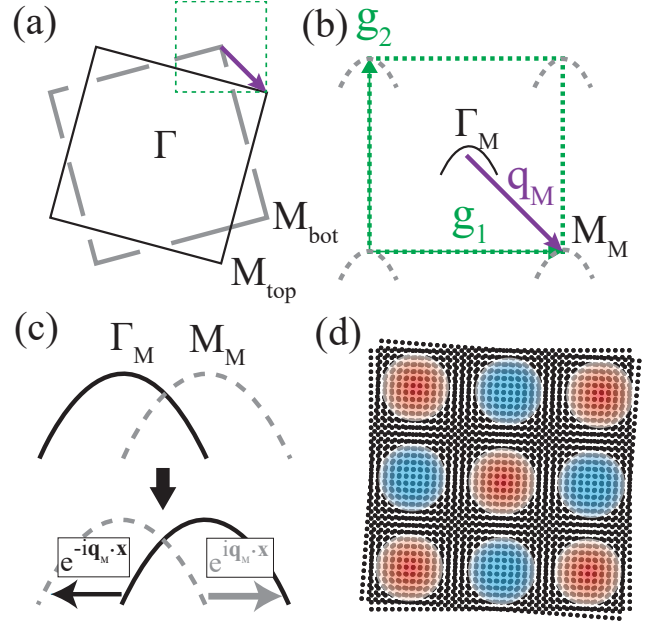


FIG. 1. (a) Momentum space of a twisted square lattice bilayer; green dashed line marks the moiré Brillouin zone near the microscopic M point. (b) Moiré Brillouin zone with marked maxima of the single-layer dispersion. (c,d) Action of the \mathcal{L} -symmetry in (c) momentum and (d) real space. (c) Layers are interchanged and then momentum of top (bottom) layer is shifted by $-(+)$ q_M . (d) The momentum shifts in (c) lead to an alternation of the wavefunction sign at AA sites, forbidding the nearest-neighbor hopping on the moiré lattice.

We will consider here the general case of flat moiré bands in twisted homobilayers of square-lattice materials using the continuum description at low twist angles. In order to obtain an effective square lattice model on the moiré scale, we must begin with electrons either at the center (Γ) or corner (M) of the original Brillouin Zone (momenta $(0, 0)$, or (π, π) , Fig. 1 (a)). Following Ref. 22 we focus on the latter (Fig. 1 (b)), since interference effects arising from valley momentum lead to more pronounced moiré patterns. A second reason, tunability of model parameters, will be discussed at length below. Un-

* paul.eugenio@uconn.edu

† zhuxi@luo@g.harvard.edu

‡ avishwanath@g.harvard.edu

§ pavel.volkov@uconn.edu

like the hexagonal counterpart [5], tight-binding calculations for twisted square Bravais lattices suggest that the flat moiré bands forming around the corner of the Brillouin zone is not described by a nearest-neighbor tight-binding model [22], raising the question of what effective models they do realize.

In this work, we reveal that the moiré bands arising near the M point of the Brillouin zone possess an approximate symmetry at low twist angles, which we refer to as \mathcal{L} -symmetry (\mathcal{L} for “layer”) (Fig. 1 (c)). This symmetry involves interchanging the bands of two layers, but does not reduce to any mirror or rotational symmetries, and thus is an emergent property of the twisted bilayer. In real space, the symmetry alternates the sign of the flat band wave-function (Fig. 1 (d)), forbidding nearest neighbor tunneling t . Interlayer displacement field or in-plane magnetic field break the \mathcal{L} -symmetry, allowing t to be continuously increased. Tuning the twist angle and displacement field allows for the realization of strongly interacting $t - t' - U$ Hubbard models with widely tunable t/t' ratios. The latter parameter plays a key role in realizing superconductivity in square lattice Hubbard [13, 40–42] and t - t' - J models [15, 43] and opens access to the frustrated spin states ([44–47] and references therein) in the Mott insulating regime.

Model: We consider a twisted bilayer of square-lattice material with band extremum (we will assume a maximum without the loss of generality) centered at the atomic zone corner $\mathbf{M} = l_a^{-1}(\pi, \pi)$, where l_a is the lattice constant (Fig. 1 (a)). The continuum Hamiltonian for the twisted bilayer near the M point can be derived similarly to previous works on graphene [48, 49] and FeSe [50] and takes the form [51]

$$H = \begin{pmatrix} h(-i\nabla_{\mathbf{x}}^{-\theta/2} + \mathbf{q}_-) & T(\mathbf{x}) \\ T(\mathbf{x})^* & h(-i\nabla_{\mathbf{x}}^{\theta/2} + \mathbf{q}_+) \end{pmatrix}, \quad (1)$$

where $h(\mathbf{k})$ is the dispersion of electrons in a single layer around M and $T(\mathbf{x}) = w_0(1 + e^{i(\mathbf{g}_1 + \mathbf{g}_2) \cdot \mathbf{x}} + e^{i\mathbf{g}_1 \cdot \mathbf{x}} + e^{i\mathbf{g}_2 \cdot \mathbf{x}})$. The moiré reciprocal lattice vectors are given by $\mathbf{g}_{1,2} = R_{\theta/2}\mathbf{G}_{1,2} - R_{-\theta/2}\mathbf{G}_{1,2}$ (where $\mathbf{G}_{1,2}$ are the reciprocal vectors of a single unrotated layer, while $\mathbf{q}_{\pm} = R_{\pm\theta/2}\mathbf{M} - \mathbf{M}$, such that the moiré Brillouin zone corner has momentum $\mathbf{q}_M \equiv \mathbf{q}_+ - \mathbf{q}_- = (\mathbf{g}_1 + \mathbf{g}_2)/2$ (Fig. 1 (b)). The moiré translation vectors are defined via $\mathbf{R}_j \cdot \mathbf{g}_k = 2\pi\delta_{jk}$.

To leading order in the twist angle, the model (1) takes a simpler form:

$$H_0 = \begin{pmatrix} \mu\nabla_{\mathbf{x}}^2 & T(\mathbf{x}) \\ T(\mathbf{x})^* & \mu(\nabla_{\mathbf{x}} + i\mathbf{q}_M)^2 \end{pmatrix}, \quad (2)$$

where the momentum origin has been shifted by $\mathbf{q}_M/2$ and we used the expansion $h(-i\nabla_{\mathbf{x}}) \approx \mu\nabla_{\mathbf{x}}^2$. Comparison between the inter-layer tunneling strength w_0 to the kinetic energy $\mu q_M^2/4$ reveals a twist angle value

$$\theta^* = \sqrt{\frac{w_0}{\frac{1}{4}\mu(\sqrt{2}\pi/l_a)^2}}, \quad (3)$$

such that emergence of isolated flat bands is expected for $\theta < \theta^*$. An example of the band structure of the model (2) for $\frac{\theta}{\theta^*} = \frac{1}{\sqrt{3}}$ is shown in Fig. 2 (a). The top band has a much smaller bandwidth W compared to others and is separated from them by a gap $E_{gap} > W$, forming an isolated flat band. Its dispersion (Fig. 2 (a), inset) fits well to a tight-binding model:

$$\epsilon_{\mathbf{k}} = -2t(\cos(k_x) + \cos(k_y)) + 2t'(\cos(k_x + k_y) + \cos(k_x - k_y)), \quad (4)$$

with t exactly equal to zero and $t' \approx 0.014w_0$. This is reflected in the eigenenergies at Γ_M and M_M points being degenerate, demonstrating a symmetry of the band under a (π, π) shift. In real space, the system separates into two decoupled moiré sublattices, consistent with the microscopic tight-binding calculations [22]. Unlike that case, the models in Eqn. (1,2) respect the full moiré translation symmetry making the emergence of sublattices surprising, and deserve further investigation.

This raises the question of whether there are symmetries of Eqn. (2) that guarantee $t = 0$ and to what extent this holds in the full Eqn.(1). Such a symmetry does exist (see Fig. 1 (c) for illustration): one can directly verify that $\hat{\mathcal{L}}^\dagger H_0 \hat{\mathcal{L}} = H_0$, where $\hat{\mathcal{L}} = \sigma_x \exp[-i\sigma_z \mathbf{q}_M \cdot \mathbf{x}]$, σ_i being Pauli matrices in layer space.

A qualitative argument as to why $\hat{\mathcal{L}}$ -symmetry forbids nearest-neighbor hopping is as follows. First, the states in the flat-band (small θ) limit are localized near AA sites, where $T(\mathbf{x}) \approx 4w_0$ is maximal, and thus approximately in the antibonding $(+1, +1)$ superposition between layers. Notice that near the centers of AA sites $\mathbf{x} = n\mathbf{R}_1 + m\mathbf{R}_2$ \mathcal{L} -symmetry reduces to $\pm\sigma_x$, where σ_x does not affect the $(+1, +1)$ state. The sign of the wavefunction therefore flips between neighboring tight-binding sites (Fig. 1 (c)), forbidding nearest-neighbor hopping.

To appreciate the scope of the symmetry noted above, we need to analyze the symmetries of the full Hamiltonian (1). This is complicated by the fact that point-group symmetries of the full system (that has D_4 point group) are realized nontrivially due to the momentum offset between two layers. As an example, consider the action of spinless time-reversal symmetry \mathcal{T} on (1). Indeed, a complex conjugation K does not bring the diagonal of Eqn. 1 into itself, reflecting that the time-reversal invariant points for two layers are different: $\mathbf{M}_{\theta/2}$ & $\mathbf{M}_{-\theta/2}$. Instead, the proper action of \mathcal{T} has to compensate for this difference resulting in $\mathcal{T} = \mathcal{U}K\mathcal{U}^\dagger = K(\mathcal{U}^\dagger)^2$, where

$$\mathcal{U} = \begin{pmatrix} e^{i\mathbf{q}_+ \cdot \mathbf{x}} & 0 \\ 0 & e^{i\mathbf{q}_- \cdot \mathbf{x}} \end{pmatrix}, \quad (5)$$

(note that $R_{\mp\theta/2}\mathbf{q}_{\pm} = -\mathbf{q}_{\mp}$ and $\mathcal{U}^\dagger = \mathcal{U}^*$). This procedure holds more generally for determining the action of any point-group operation g on Eqn. (1), i.e $\mathcal{U}g\mathcal{U}^\dagger$ – see supplementary material for details [51].

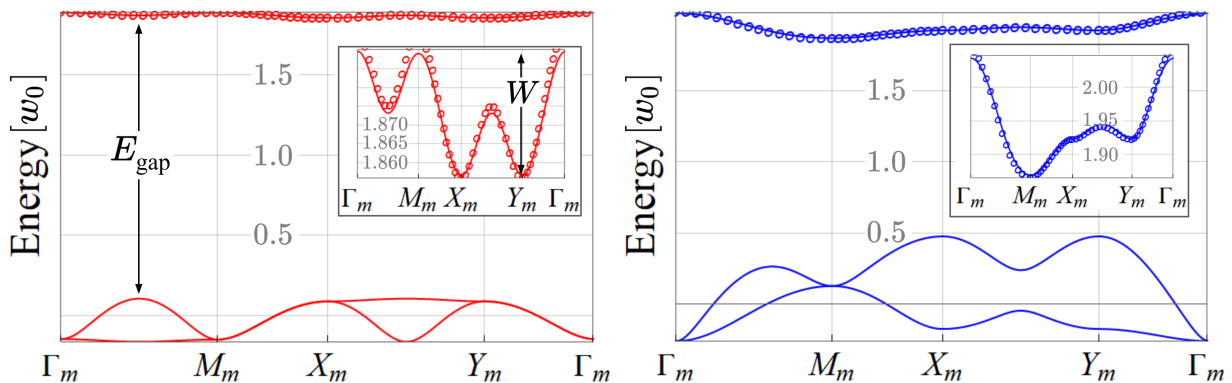


FIG. 2. (a) Band structure (in units of interlayer tunneling amplitude w_0) of the model Eq. (2) with $\theta/\theta^* = 1/\sqrt{3}$ and (b) with an additional inter-layer displacement field $V = 5V_c$ (11). Insets show the details of the top flat band, separated by E_{gap} from the rest. Note, the degeneracy between bands separated by momentum (π, π) is removed in the right inset. Numerical results using plane-wave expansion are shown as continuous lines. Circles represent the analytic tight-binding model for the top band – see Eqn’s 4, 8, & 9; for (a) we find $t = 0$, $t' \approx 0.014w_0$, while in (b) we find $t \approx 0.07$, $t' \approx 0.014w_0$ giving $t/t' = 5$.

The above suggests that all point-group operations will be realized conventionally (as just g) after the following unitary transformation of (1):

$$H_f = U^\dagger H U = \begin{pmatrix} h(-i\nabla_{\mathbf{x}}^{-\theta/2}) & U(\mathbf{x}) \\ U(\mathbf{x}) & h(-i\nabla_{\mathbf{x}}^{\theta/2}) \end{pmatrix}, \quad (6)$$

where $U(\mathbf{x}) = 2w_0 \left(\cos\left(\frac{\mathbf{g}_1 + \mathbf{g}_2}{2} \cdot \mathbf{x}\right) + \cos\left(\frac{\mathbf{g}_1 - \mathbf{g}_2}{2} \cdot \mathbf{x}\right) \right)$. The moiré translation symmetry is represented as $T_{\mathbf{R}_{1,2}} = e^{i\mathbf{q} + \mathbf{R}_{1,2}} \sigma_z e^{\mathbf{R}_{1,2} \cdot \nabla_{\mathbf{x}}}$ in this case.

Neglecting the rotation of the intralayer dispersion (discussed below) $h(-i\nabla_{\mathbf{x}}^{\pm\theta/2}) \rightarrow h(-i\nabla_{\mathbf{x}})$, the \mathcal{L} -symmetry emerges in (6) as $[H_f, \sigma_x] = 0$. This symmetry implies that (6) can be diagonalized with bonding/antibonding states of the form $(1, \pm 1)^T \psi_{\pm}(\mathbf{x})$, where

$$\left(\mu \nabla_{\mathbf{x}}^2 \pm U(\mathbf{x}) \right) \psi_{\pm}(\mathbf{x}) = E \psi_{\pm}(\mathbf{x}). \quad (7)$$

Taking into account $U(\mathbf{x} + \mathbf{R}_1) = -U(\mathbf{x})$, implies that: (i) the eigen-energies of the \pm sectors are degenerate (ii) the eigenstates of the sectors are related via a translation by a moiré site. Therefore, the eigenstates of (6) form two degenerate decoupled bands with Wannier functions localized on two different sublattices of the moiré lattice. In the tight-binding language all hoppings between the two sublattices vanish exactly in this case, explaining the structure of the bands in Fig. 2 (a).

Let us now discuss the relation of the \mathcal{L} -symmetry to microscopic symmetries of the twisted bilayer. Eq. (7) appears to possess all elements of the D_{4h} point group of the untwisted bilayer. However, the \mathcal{L} -symmetry operation σ_x does not commute with the translations $T_{\mathbf{R}_{1,2}}$ (containing σ_z in this representation), which is notably distinct from the $z \rightarrow -z$ mirror symmetry of the $\theta = 0$ bilayer. There are also two exact symmetries of Eqn. 6 which do interchange layers - 180° rotations about in-

plane axes C'_2 & C''_2 . These are also distinct from the \mathcal{L} -symmetry, as they act on the coordinates \mathbf{x} . This implies that for small twist angles, the M-point flat bands are characterized by an approximate symmetry group that is distinct from (and not a subgroup of) the space group of the twisted bilayer. The approximate symmetry enforces the unexpected pattern of band degeneracies.

The rotations of momenta $i\nabla_{\mathbf{x}}^{\pm\theta/2}$ in Eq. (6) break the \mathcal{L} -symmetry, reducing the point-group to D_4 , which is the appropriate point-group for the twisted bilayer. However, the \mathcal{L} -breaking corrections only arise in the 4th order in the expansion of $h(\mathbf{k})$ in \mathbf{k} : $\delta h(\mathbf{k}) \propto \theta k_x k_y (k_x^2 - k_y^2) \sigma_z$. Their magnitude is of the order $\mathcal{O}(\theta^5)$, demonstrating that the \mathcal{L} -symmetry is remarkably robust. We note that in addition to the terms considered in (1), the twisted layers also produce an electrostatic potential that amounts to a term $U_0(\mathbf{x}) \sigma_0$ [5, 32], that is periodic under a moiré translation. This term does not change any of the arguments above and does not break the \mathcal{L} -symmetry. If the magnitude of this term is smaller than E_{gap} , it will not alter the band structure described here qualitatively and we thus leave the detailed study of the effects of $U_0(\mathbf{x})$ to future work.

Tunable intersublattice coupling: Identifying the \mathcal{L} -symmetry as the origin of emergent decoupled sublattices opens the possibility to create a tunable coupling between them by introducing layer asymmetry. For electronic systems, this can be achieved either with a displacement field $V\sigma_z$ or with the orbital effect of an in-plane magnetic field. The latter introduced by modifying Eq 6: $-i\nabla_{\mathbf{x}} \rightarrow -i\nabla_{\mathbf{x}} - \frac{e_0}{2c} \mathbf{B} d_{\parallel} \sigma_z$ [52], where d_{\parallel} is the distance between two layers and e_0 is the electron charge. Both of these terms mix the bonding and antibonding eigenstates of Eq. (7). Thus, in the Wannier basis, these terms would generate nearest-neighbor hopping.

To illustrate the effect of V , we numerically computed the spectrum of the Hamiltonian for θ where the band is isolated and flat (Fig 2(a)), then turned on V (Fig

2(b)) without changing θ . Though the chosen value of V is sizable enough to guarantee the band is well fit by (4) with $t/t' = 5$, the band remains flat and isolated. Physically, Eqn. 6 can be interpreted as a lattice with a layer isospin, and an applied isospin Zeeman field $\pm\hat{x}$, that is staggered between opposite sublattices. Fermions are therefore restricted to hop on the same sublattice, unless an inter-layer electric field (isospin field $\pm\hat{z}$) is switched on. The latter leads to ‘canting’ of the isospin, and permits hopping between sublattices.

Expressions for t & t' in Eq. (4) can be obtained using exact solutions of Eqn. (7) assuming that $W, V \ll E_{\text{gap}}$ such that Eqn. (4) holds. After variable separation along orthogonal lines connecting next-to-nearest neighbor sites of the moiré lattice, i.e $\psi_{\pm}(\mathbf{x}) = \psi_{X,\pm}(\frac{x+y}{\sqrt{2}})\psi_{Y,\pm}(\frac{x-y}{\sqrt{2}})$, Eqn (7) reduces to 1D Mathieu equations for which exact and asymptotic solutions are known [51, 53]. The expression for t' is given by [51]:

$$t' = \frac{w_0\theta^2}{4\theta^{*2}} f_{t'}\left(\frac{\theta^*}{\theta}\right) \approx_{\theta \ll \theta^*} w_0 \frac{4^{7/4}}{\sqrt{\pi}} \left(\frac{\theta}{\theta^*}\right)^{1/2} e^{-4\frac{\theta^*}{\theta}} \quad (8)$$

where $f_{t'}(z) = a_1(1, z^2) - a_1(0, z^2)$, a_1 being the characteristic value of the 1D Mathieu equation.

In presence of finite V , eigenstates of Eq. (7) split at $\mathbf{k} = 0$ by $\Delta E(\mathbf{k} = 0) = 2V\langle\psi_+^{\mathbf{k}=0}|\psi_-^{\mathbf{k}=0}\rangle$. Since (5) folds the $\mathbf{\Gamma}_M$ and \mathbf{M}_M points onto one another, this splitting is equal to $8t$ (see (4)). The wavefunction overlap can be obtained from Mathieu functions or using WKB approximation for $\theta \ll \theta^*$ [51, 53, 54]:

$$t = \frac{Vg_t^2\left(\frac{\theta^*}{\theta}\right)}{\pi^2} \approx_{\theta \ll \theta^*} V \frac{\tan^2\left(\frac{\pi}{8}\right)}{2^{-7/2}} e^{-4(2-\sqrt{2})\frac{\theta^*}{\theta}}. \quad (9)$$

where $g_t(z) = \int_0^\pi dx ce_0(x, z) ce_1(x + \pi/2, z)$, ce_0 being the periodic Mathieu functions [51].

A similar approach allows us to understand the orbital effect of an in-plane magnetic field $\mathbf{B} \neq 0$. In particular, the nearest-neighbor hopping in first order in B takes the form $t_B = i\frac{\mu\epsilon_0}{c}d_{\parallel}\langle W_+(\mathbf{x})|(\mathbf{B} \cdot \nabla)|W_-(\mathbf{x})\rangle$, where we use $|W_{\pm}(\mathbf{x})\rangle$ to denote the Wannier functions of the Mathieu solutions. The overlap integrals can be computed with WKB method [51] and yield an anisotropic hopping:

$$t_{x/y} \approx i4\sqrt{\mu w_0} \frac{e_0 B_{x/y} d_{\parallel}}{2c} \frac{\tan^2\left(\frac{\pi}{8}\right)}{2^{-7/2}} e^{-4(2-\sqrt{2})\frac{\theta^*}{\theta}}. \quad (10)$$

The relative effect of this term compared to that of V can be estimated as $t_{x/y}^B/t^V \sim \frac{w_0\theta}{V\theta^*} \frac{Bd_{\parallel}l_a}{\theta\Phi_0}$, where the second term is the magnetic flux per lateral moiré unit cell which can reach values ~ 0.1 for fields ~ 10 T and $d \sim 1$ nm, $l_a/\theta \sim 10$ nm. For systems with large enough w_0 this is sufficient to introduce weak anisotropy. Note however, that the exponential dependence on θ is weaker for $t_{x/y}$ than for t' , and therefore its effect may become comparable to bandwidth at low enough twist angles.

$t - t' - U$ Hubbard models: We now demonstrate that these results allow twisted bilayers of square lattice materials to realize the physics of t-t'-U Hubbard

model in strongly correlated regime with a widely tunable t/t' ratio. The bandwidth of the flat band $W = \max\{4t + 8t', 8t\}$ can be seen from Eqns. (8,9) to be exponentially small at $\theta < \theta^*$. The gap to the remote bands E_{gap} , on the other hand, follows $4w_0\theta/\theta^*$ in this regime (obtained from expansion of (6) near AA sites [51]), demonstrating that the flat band is well isolated.

We can estimate now the displacement field strength needed to tune the t/t' ratio in a wide range. Consider the value V_c , where nearest-neighbor tunneling becomes comparable to the next-nearest neighbor $t(V_c)/t' = 1$:

$$V_c = \frac{t'}{(t/V)} \approx w_0 \frac{\sqrt{\theta/\theta^*}}{\tan^2(\frac{\pi}{8})\sqrt{\pi}} e^{-4(\sqrt{2}-1)\frac{\theta^*}{\theta}}. \quad (11)$$

Crucially, $V_c(\theta)$ is an exponential function of θ ; therefore, displacement fields much smaller than the band gap $V \ll E_{\text{gap}}$ are sufficient to induce strong nearest neighbor hopping, retaining the isolated flat band.

The effects of Coulomb interactions can be estimated in the limit $\theta \ll \theta^*$, where states are localized near AA sites. The projected Coulomb interaction between two electrons at sites separated by a distance r is given by [51] $U(r) = \frac{e_0^2}{4\pi\epsilon} \frac{\pi^{1/2}}{32l_o} e^{-\frac{l_o^2 r^2}{2}} I_0\left(\frac{l_o^{-2} r^2}{2}\right)$, where $l_o = \sqrt{2}(\mu w_0^{-1})^{1/4} q_M^{-1/2}$, is the wave-function spread and ϵ is the permittivity, which can be controlled through screening via an electrostatic gate [8]. $I_0(\mathbf{x}) \equiv J_0(i\mathbf{x})$ is the modified Bessel function of the first kind, the asymptotic expansion of which tells us $U(r) \sim 1/(2r)$. Off-site interactions are thus proportional to θ at low twist angles. However, the on-site interaction energy ($r = 0$),

$$U_0 = \frac{e_0^2}{4\pi\epsilon l_a} \frac{\pi^{3/2}}{2^{3/2}} \sqrt{\theta\theta^*}, \quad (12)$$

is parametrically larger, suggesting that a Hubbard-like description is appropriate at low θ .

We summarize the energy scales discussed above as a function of twist angle in Fig. 3, where they are obtained from exact solutions of Eq. 7 using Mathieu functions [51]. The results demonstrate that for $\theta \ll \theta^*$, an isolated flat band emerges $E_{\text{gap}} \gg W$. A lower bound estimate of the correlation strength is obtained by noting that the ratio: $U(\theta = \theta^*)/w_0$ is related to r_s^* , the dimensionless Coulomb electron correlation parameter for a single layer at density $(\theta^*/l_a)^2$ in the moiré-less limit, $\frac{U(\theta=\theta^*)}{w_0} \approx \frac{r_s^*}{\sqrt{8\pi}}$. Moreover at low θ , W is exponentially suppressed (8,9) in contrast to the interaction (12), leading to the strongly interacting regime $U_0 \gg W$. Finally, the relevant value of displacement field V_c (11) is suppressed exponentially at low θ , guaranteeing $W(V_c) \ll E_{\text{gap}}$ as $\theta \rightarrow 0$. Thus the band will remain flat and isolated even when t is dominant, such as is demonstrated in Fig 2 (b) where $t/t' = 5$. Controlling θ & V allows to traverse the entire t'/t phase diagram of the Hubbard mode while remaining in the strong coupling regime.

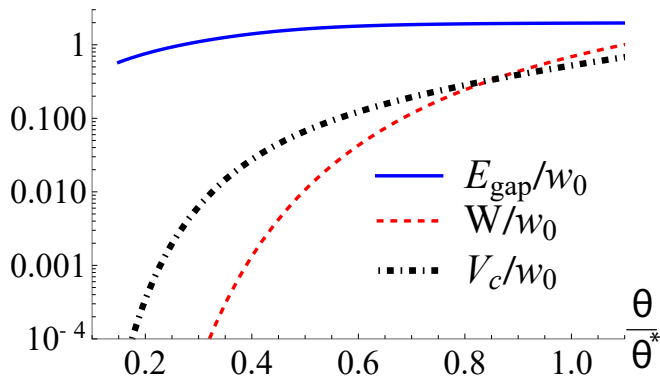


FIG. 3. Dependence of the moiré flat band parameters [Fig. 2] on θ : gap to the remote bands (E_{gap}), bandwidth (W with $V = 0$) and displacement field necessary to achieve $t/t' = 1$ (V_c , Eq. 11), all normalized to the inter-layer tunneling w_0 . At $\theta < \theta^*$ $E_{\text{gap}} \gg W, V_c$, such that an isolated flat band with widely tunable t'/t is realized.

Discussion and Outlook: The \mathcal{L} -symmetry and its consequences arise from the interference of the electron waves arising from the vicinity of M point of individual monolayers. This can be contrasted with moiré bands formed from layer fields originating near Γ [32], where twist does not create a momentum shift between the band extrema. The dominant term in the tunneling is then just a constant, favoring a homogeneous bonding/antibonding state with a usual tight-binding description that should have $t \gg t'$.

The ability to control the ratio t'/t and U/t is critical for correlated electron physics. The ratio t'/t is believed to be crucial for realizing superconductivity in square lattice Hubbard [13, 40–42] and t - t' - J models [15, 43], to the extent that for $t' = 0$ no superconductivity appears [13, 14]. The exploration of a wide range of t'/t ratios may therefore test the ultimate bounds on T_c in the Hubbard model. Furthermore, The Hubbard model for $t'/t \sim 1$ has been argued to exhibit a number of exotic phenomena, including a topological $d_{x^2-y^2} \pm id_{xy}$ pairing state [55, 56]. Also, in the Mott insulating regime at half filling, the effective description of the system becomes the J - J' Heisenberg model, with J'/J is set by the ratio of t'/t . In the frustrated regime $J'/J \approx 0.5$, there

is an open question as to the existence of a potential spin liquid phase and its character [44–47] - the system we propose would allow traversing this phase as a function of gate voltage. Finally, the controlled spatial anisotropy induced by an in-plane magnetic field can help clarify the role of nematic order on the square lattice.

We stress that our proposal requires neither special band touching nor non-trivial topology for individual layers utilizing instead the conventional band extremum at the Brillouin zone corner expected in generic atomic tight-binding models. Monolayer square lattice materials include currently cuprates [57] as well as monolayer FeSe [58, 59] and FeS [60]. Both FeSe & FeS monolayers having been shown to have small Fermi surfaces about M . Other candidate platforms deriving from exfoliable materials [3], will be discussed in a separate publication [61]. Finally, our main predictions of the emergent sublattice symmetry can be tested in analogue simulators, such as cold atoms [33–35], optical [36–38] and acoustic [39] metamaterials by studying the wave propagation from a state localized on one sublattice only.

To conclude, we have demonstrated the existence of an approximate \mathcal{L} -symmetry in twisted square lattices that results in an emergent sublattice structure for the flat bands. The sublattices can be coupled on demand by introducing layer asymmetry with external fields. Our results open the path towards the realization of electronic $t - t' - U$ Hubbard model physics with a widely tunable t'/t ratio. More generally, we demonstrated the important role that emergent symmetries beyond the space group can play in moiré systems.

ACKNOWLEDGMENTS

We thank Leon Balents and Donna N. Sheng for comments and discussion. A. V. would like to thank Toshikaze Kariyado for an earlier related collaboration and for discussions. This research was supported in part by the Simons Collaboration on Ultra-Quantum Matter which is a grant from the Simons Foundation (651440, Z.-X. L.) and by the Center for Advancement of Topological Semimetals, an Energy Frontier Research Center funded by the US Department of Energy Office of Science, Office of Basic Energy Sciences, through the Ames Laboratory under contract No. DEAC02-07CH11358.

-
- [1] Y. Liu, N. O. Weiss, X. Duan, H.-C. Cheng, Y. Huang, and X. Duan, Van der waals heterostructures and devices, *Nature Reviews Materials* **1**, 1 (2016).
 [2] K. S. Novoselov, A. Mishchenko, A. Carvalho, and A. H. C. Neto, 2d materials and van der waals heterostructures, *Science* **353**, aac9439 (2016), <https://www.science.org/doi/pdf/10.1126/science.aac9439>.
 [3] N. Mounet, M. Gibertini, P. Schwaller, D. Campi, A. Merkys, A. Marrazzo, T. Sohier, I. E. Castelli, A. Ce-

- pellotti, G. Pizzi, and N. Marzari, Two-dimensional materials from high-throughput computational exfoliation of experimentally known compounds, *Nature Nanotechnology* **13**, 246–252 (2018).
 [4] L. Balents, C. R. Dean, D. K. Efetov, and A. F. Young, Superconductivity and strong correlations in moiré flat bands, *Nat. Phys.* **16**, 725 (2020).
 [5] F. Wu, T. Lovorn, E. Tutuc, and A. H. MacDonald, Hubbard model physics in transition metal dichalcogenide

- moiré bands, *Phys. Rev. Lett.* **121**, 026402 (2018).
- [6] Y. Tang, L. Li, T. Li, Y. Xu, S. Liu, K. Barmak, K. Watanabe, T. Taniguchi, A. H. MacDonald, J. Shan, et al., Simulation of hubbard model physics in wse2/ws2 moiré superlattices, *Nature* **579**, 353 (2020).
- [7] K. S. Burch, D. Mandrus, and J.-G. Park, Magnetism in two-dimensional van der waals materials, *Nature* **563**, 47 (2018).
- [8] X. Liu, Z. Wang, K. Watanabe, T. Taniguchi, O. Vafek, and J. I. A. Li, Tuning electron correlation in magic-angle twisted bilayer graphene using coulomb screening, *Science* **371**, 1261 (2021), <https://www.science.org/doi/pdf/10.1126/science.abb8754>.
- [9] D. M. Kennes, M. Claassen, L. Xian, A. Georges, A. J. Millis, J. Hone, C. R. Dean, D. N. Basov, A. N. Pasupathy, and A. Rubio, Moiré heterostructures as a condensed-matter quantum simulator, *Nature Physics* **17**, 155 (2021).
- [10] Y. Deng, E. Kozik, N. V. Prokof'ev, and B. V. Svistunov, Emergent bcs regime of the two-dimensional fermionic hubbard model: Ground-state phase diagram, *Europhysics Letters* **110**, 57001 (2015).
- [11] E. W. Huang, C. B. Mendl, S. Liu, S. Johnston, H.-C. Jiang, B. Moritz, and T. P. Devereaux, Numerical evidence of fluctuating stripes in the normal state of high- T_c cuprate superconductors, *Science* **358**, 1161 (2017).
- [12] B.-X. Zheng, C.-M. Chung, P. Corboz, G. Ehlers, M.-P. Qin, R. M. Noack, H. Shi, S. R. White, S. Zhang, and G. K.-L. Chan, Stripe order in the underdoped region of the two-dimensional hubbard model, *Science* **358**, 1155 (2017).
- [13] H.-C. Jiang and T. P. Devereaux, Superconductivity in the doped hubbard model and its interplay with next-nearest hopping t' , *Science* **365**, 1424 (2019).
- [14] M. Qin, C.-M. Chung, H. Shi, E. Vitali, C. Hubig, U. Schollwöck, S. R. White, and S. Zhang (Simons Collaboration on the Many-Electron Problem), Absence of superconductivity in the pure two-dimensional hubbard model, *Phys. Rev. X* **10**, 031016 (2020).
- [15] S. Jiang, D. J. Scalapino, and S. R. White, Ground-state phase diagram of the $t-t'$ model, *Proceedings of the National Academy of Sciences* **118**, e2109978118 (2021), <https://www.pnas.org/doi/pdf/10.1073/pnas.2109978118>.
- [16] M. Qin, T. Schäfer, S. Andergassen, P. Corboz, and E. Gull, The hubbard model: A computational perspective, *Annual Review of Condensed Matter Physics* **13**, 275 (2022).
- [17] D. P. Arovas, E. Berg, S. A. Kivelson, and S. Raghu, The hubbard model, *Annual Review of Condensed Matter Physics* **13**, 239 (2022).
- [18] V. Anisimov, D. Bukhvalov, and T. Rice, Electronic structure of possible nickelate analogs to the cuprates, *Physical Review B* **59**, 7901 (1999).
- [19] G. A. Pan, D. Ferenc Segedin, H. LaBollita, Q. Song, E. M. Nica, B. H. Goodge, A. T. Pierce, S. Doyle, S. Novakov, D. Córdoba Carrizales, A. T. N'Diaye, P. Shafer, H. Paik, J. T. Heron, J. A. Mason, A. Yacoby, L. F. Kourkoutis, O. Erten, C. M. Brooks, A. S. Botana, and J. A. Mundy, Superconductivity in a quintuple-layer square-planar nickelate, *Nature Materials* **21**, 160 (2022).
- [20] D. Li, K. Lee, B. Y. Wang, M. Osada, S. Crossley, H. R. Lee, Y. Cui, Y. Hikita, and H. Y. Hwang, Superconductivity in an infinite-layer nickelate, *Nature* **572**, 624 (2019).
- [21] A. Bohrdt, L. Homeier, C. Reinmoser, E. Demler, and F. Grusdt, Exploration of doped quantum magnets with ultracold atoms, *Annals of Physics* **435**, 168651 (2021), special issue on Philip W. Anderson.
- [22] T. Kariyado and A. Vishwanath, Flat band in twisted bilayer bravais lattices, *Phys. Rev. Res.* **1**, 033076 (2019).
- [23] Z.-X. Luo, C. Xu, and C.-M. Jian, Magic continuum in a twisted bilayer square lattice with staggered flux, *Phys. Rev. B* **104**, 035136 (2021).
- [24] Y. Soeda, K. Asaga, and T. Fukui, Moiré landau levels of a C_4 -symmetric twisted bilayer system in the absence of a magnetic field, *Phys. Rev. B* **105**, 165422 (2022).
- [25] M.-R. Li, A.-L. He, and H. Yao, Magic-angle twisted bilayer systems with quadratic band touching: Exactly flat bands with high chern number, *Phys. Rev. Res.* **4**, 043151 (2022).
- [26] O. Can, T. Tummuru, R. P. Day, I. Elfimov, A. Damascelli, and M. Franz, High-temperature topological superconductivity in twisted double-layer copper oxides, *Nature Physics* **17**, 519–524 (2021).
- [27] S. F. Zhao, X. Cui, P. A. Volkov, H. Yoo, S. Lee, J. A. Gardener, A. J. Akey, R. Engelke, Y. Ronen, R. Zhong, et al., Time-reversal symmetry breaking superconductivity between twisted cuprate superconductors, *Science* **382**, 1422 (2023).
- [28] X.-Y. Song, Y.-H. Zhang, and A. Vishwanath, Doping a moiré mott insulator: A $t-j$ model study of twisted cuprates, *Phys. Rev. B* **105**, L201102 (2022).
- [29] R. Haenel, T. Tummuru, and M. Franz, Incoherent tunneling and topological superconductivity in twisted cuprate bilayers, *Phys. Rev. B* **106**, 104505 (2022).
- [30] P. A. Volkov, J. H. Wilson, K. P. Lucht, and J. H. Pixley, Magic angles and correlations in twisted nodal superconductors, *Phys. Rev. B* **107**, 174506 (2023).
- [31] P. A. Volkov, J. H. Wilson, K. P. Lucht, and J. H. Pixley, Current- and field-induced topology in twisted nodal superconductors, *Phys. Rev. Lett.* **130**, 186001 (2023).
- [32] P. M. Eugenio and O. Vafek, Twisted-bilayer FeSe and the Fe-based superlattices, *SciPost Phys.* **15**, 081 (2023).
- [33] A. González-Tudela and J. I. Cirac, Cold atoms in twisted-bilayer optical potentials, *Phys. Rev. A* **100**, 053604 (2019).
- [34] T. Salamon, A. Celi, R. W. Chhajlany, I. Frérot, M. Lewenstein, L. Tarruell, and D. Rakshit, Simulating twistrionics without a twist, *Phys. Rev. Lett.* **125**, 030504 (2020).
- [35] Z. Meng, L. Wang, W. Han, F. Liu, K. Wen, C. Gao, P. Wang, C. Chin, and J. Zhang, Atomic bose-einstein condensate in twisted-bilayer optical lattices, *Nature* **615**, 231 (2023).
- [36] Q. Fu, P. Wang, C. Huang, Y. V. Kartashov, L. Torner, V. V. Konotop, and F. Ye, Optical soliton formation controlled by angle twisting in photonic moiré lattices, *Nature Photonics* **14**, 663 (2020).
- [37] P. Wang, Y. Zheng, X. Chen, C. Huang, Y. V. Kartashov, L. Torner, V. V. Konotop, and F. Ye, Localization and delocalization of light in photonic moiré lattices, *Nature* **577**, 42 (2020).
- [38] B. Lou, N. Zhao, M. Minkov, C. Guo, M. Orenstein, and S. Fan, Theory for twisted bilayer photonic crystal slabs, *Phys. Rev. Lett.* **126**, 136101 (2021).
- [39] Z. Jiang, J. Liu, S. Zheng, G. Duan, and B. Xia, Phononic twisted moiré lattice with quasicrys-

- talline patterns, *Applied Physics Letters* **121**, 142202 (2022), <https://pubs.aip.org/aip/apl/article-pdf/doi/10.1063/5.0109404/16483255/142202.1.online.pdf>.
- [40] C.-M. Chung, M. Qin, S. Zhang, U. Schollwöck, and S. R. White (The Simons Collaboration on the Many-Electron Problem), Plaquette versus ordinary d -wave pairing in the t' -hubbard model on a width-4 cylinder, *Phys. Rev. B* **102**, 041106 (2020).
- [41] Y.-F. Jiang, J. Zaanen, T. P. Devereaux, and H.-C. Jiang, Ground state phase diagram of the doped hubbard model on the four-leg cylinder, *Phys. Rev. Res.* **2**, 033073 (2020).
- [42] M. Danilov, E. G. van Loon, S. Brener, S. Isakov, M. I. Katsnelson, and A. I. Lichtenstein, Degenerate plaquette physics as key ingredient of high-temperature superconductivity in cuprates, *npj Quantum Materials* **7**, 50 (2022).
- [43] X. Lu, F. Chen, W. Zhu, D. N. Sheng, and S.-S. Gong, Emergent superconductivity and competing charge orders in hole-doped square-lattice t - j model, *Phys. Rev. Lett.* **132**, 066002 (2024).
- [44] H.-C. Jiang, H. Yao, and L. Balents, Spin liquid ground state of the spin- $\frac{1}{2}$ square J_1 - J_2 heisenberg model, *Phys. Rev. B* **86**, 024424 (2012).
- [45] Y. Nomura and M. Imada, Dirac-type nodal spin liquid revealed by refined quantum many-body solver using neural-network wave function, correlation ratio, and level spectroscopy, *Phys. Rev. X* **11**, 031034 (2021).
- [46] X. Qian and M. Qin, Absence of spin liquid phase in the $J_1 - J_2$ heisenberg model on the square lattice, *Phys. Rev. B* **109**, L161103 (2024).
- [47] A. Rückriegel, D. Tarasevych, and P. Kopietz, Phase diagram of the j_1 - j_2 quantum heisenberg model for arbitrary spin (2024), [arXiv:2403.08713 \[cond-mat.str-el\]](https://arxiv.org/abs/2403.08713).
- [48] R. Bistritzer and A. H. MacDonald, Moiré bands in twisted double-layer graphene, *Proceedings of the National Academy of Sciences* **108**, 12233 (2011).
- [49] L. Balents, General continuum model for twisted bilayer graphene and arbitrary smooth deformations, *SciPost Phys.* **7**, 048 (2019).
- [50] P. M. Eugenio and O. Vafek, Twisted-bilayer FeSe and the Fe-based superlattices, *SciPost Phys.* **15**, 081 (2023).
- [51] See Supplementary Materials.
- [52] The Zeeman effect simply produces a spin splitting in this case.
- [53] G. Catelani, R. J. Schoelkopf, M. H. Devoret, and L. I. Glazman, Relaxation and frequency shifts induced by quasiparticles in superconducting qubits, *Phys. Rev. B* **84**, 064517 (2011).
- [54] M. Arzamasovs and B. Liu, Tight-binding tunneling amplitude of an optical lattice, *European Journal of Physics* **38**, 065405 (2017).
- [55] S. Sachdev, Quantum phase transitions of correlated electrons in two dimensions, *Physica A: Statistical Mechanics and its Applications* **313**, 252 (2002), *Fundamental Problems in Statistical Physics*.
- [56] E. M. Nica and Q. Si, Multiorbital singlet pairing and $d+d$ superconductivity, *npj Quantum Materials* **6**, 3 (2021).
- [57] Y. Yu, L. Ma, P. Cai, R. Zhong, C. Ye, J. Shen, G. D. Gu, X. H. Chen, and Y. Zhang, High-temperature superconductivity in monolayer $\text{Bi}_2\text{Sr}_2\text{CaCu}_2\text{O}_{8+\delta}$, *Nature* **575**, 156 (2019).
- [58] S. Kanayama, K. Nakayama, G. N. Phan, M. Kuno, K. Sugawara, T. Takahashi, and T. Sato, Two-dimensional dirac semimetal phase in undoped one-monolayer FeSe film, *Phys. Rev. B* **96**, 220509 (2017).
- [59] Y. Zhang, J. J. Lee, R. G. Moore, W. Li, M. Yi, M. Hashimoto, D. H. Lu, T. P. Devereaux, D.-H. Lee, and Z.-X. Shen, Superconducting gap anisotropy in monolayer FeSe thin film, *Phys. Rev. Lett.* **117**, 117001 (2016).
- [60] K. Shigekawa, K. Nakayama, M. Kuno, G. N. Phan, K. Owada, K. Sugawara, T. Takahashi, and T. Sato, Dichotomy of superconductivity between monolayer fese and fese, *Proceedings of the National Academy of Sciences* **116**, 24470 (2019).
- [61] Z. Luo et al., in preparation.
- [62] J. Kang and O. Vafek, Symmetry, maximally localized wannier states, and a low-energy model for twisted bilayer graphene narrow bands, *Phys. Rev. X* **8**, 031088 (2018).
- [63] O. Vafek and J. Kang, Continuum effective hamiltonian for graphene bilayers for an arbitrary smooth lattice deformation from microscopic theories, *Phys. Rev. B* **107**, 075123 (2023).

Supplemental Material

CONTENTS

Acknowledgments	5
References	5
A. A minimal picture of moiré tunneling	8
1. Boosts and the action of symmetries in different representations	8
2. Boosts by rotating a crystal	9
3. Deriving the local field theories from microscopies	11
4. Moiré periodicity isn't the commensurate one	13
B. Tight-binding in the asymptotic limit of small θ	14
1. Notation	14
2. Lattice of harmonic oscillators	14
3. Mathieu equation and wavefunctions	15
4. Wannier orbitals and tight-binding formalism	16
a. Hoppings: t, t' , & $t_{x/y}$	17
5. WKB derivation of the overlaps	19
a. Overlap \mathcal{O}_0	20
b. Overlap of the gradient \mathcal{O}_1	20

This supplementary material is organized as follows. In Sec. A we present a detailed derivation of Eq. 1 in the main text and discuss the realization of symmetries. In Sec. B, we present details of the calculations for Eqs. 8-12 in the main text for the low twist angle limit.

Appendix A: A minimal picture of moiré tunneling

In the following subsections, we present a derivation of the moiré tunneling from the perspective of effective field theory and symmetry. The purpose of this presentation is to provide the reader with a top-down (starting from long-wavelength field theories) understanding of moiré, as opposed to bottom-up (starting from microscopies). The value in this minimal picture is that it highlights the essential ingredients leading to the emergence of periodicity in a system where microscopically no translation symmetry exists. In other words, we wish to answer the questions: What ingredients in the low energy description must be present in order for moiré periodicity to emerge at arbitrary non-commensurate θ ? What does this low-energy description reveal to us about the sublattice structure governed by \mathcal{L} -symmetry? And at small θ , what are the irrelevant processes that are responsible for the microscopic breaking of translation?

1. Boosts and the action of symmetries in different representations

To start, consider a field theory with Hamiltonian $h(\hat{\mathbf{p}}) = \hat{\mathbf{p}}^2$, which we argue to be the accurate low-energy description of a hypothetical system (a “layer”). For simplicity, we will consider no spin nor valley degrees of freedom, such that h labels all relevant low-energy degrees of freedom. When we say that our layer has a symmetry, we mean that there is an operation \hat{O} that leaves h invariant, i.e $\hat{O}^{-1}h\hat{O} = h$ or equivalently $[\hat{O}, h] = 0$. One such operation is time-reversal \mathcal{T} , which by construction is an operation which reverses the motion of the system. This motion is described by $\hat{\mathbf{p}} = -i\nabla$, which is the generator of translation. Since \mathcal{T} leaves position invariant, this tells us that in order for $\mathcal{T}^{-1}\hat{\mathbf{p}}\mathcal{T} = -\hat{\mathbf{p}}$ one has to have $\mathcal{T} = K$ where K is complex conjugation.

The reason we are concerned with symmetries of the Hamiltonian, as opposed to other operators, is because the Hamiltonian is the generator of time evolution, i.e $i\partial_t|\psi\rangle = h|\psi\rangle$, and therefore governs the system dynamics. Its eigenenergies provide a convenient characterization of a system, because they are by definition a quantity which is

held invariant under shifts in time, i.e $[\exp(-i\delta t h), h] \equiv 0$. So that for a system described by wavefunction $|\psi(t)\rangle$ and constant h ,

$$\langle \psi(t + \delta t) | h | \psi(t + \delta t) \rangle = \langle \psi(t) | e^{i\delta t h} h e^{-i\delta t h} | \psi(t) \rangle = \langle \psi(t) | h | \psi(t) \rangle,$$

which tells us it doesn't matter if we measure the energy first, or wait to measure – the average energy remains the same. Likewise, observables whose corresponding operations commute with h inherit this property, such that their eigenvalues label the system's steady states.

Consider now the unitary transformation $|\psi\rangle = \exp(i\mathbf{q}\cdot\mathbf{x})|\tilde{\psi}\rangle$, with constant vector \mathbf{q} , which has the effect of bringing us into a representation of our system whose wavefunction evolves via $i\partial_t|\tilde{\psi}\rangle = h(\hat{\mathbf{p}} + \mathbf{q})|\tilde{\psi}\rangle$. Such a Hamiltonian appears to describe a system whose center of momentum has been shifted to $-\mathbf{q}$. We may therefore feel obliged to relabel the total momentum as the operator $\hat{\Pi} = \hat{\mathbf{p}} + \mathbf{q}$, and likewise expect $\mathcal{T}^{-1}\hat{\Pi}\mathcal{T} = -\hat{\Pi}$. However, if we take $\mathcal{T} = K$ as before, this does not work, because \mathbf{q} is a real-valued vector which does not change sign under complex conjugation. This has the important consequence that $K^{-1}h(\hat{\mathbf{p}} + \mathbf{q})K = h(-\hat{\mathbf{p}} + \mathbf{q}) \neq h(\hat{\mathbf{p}} + \mathbf{q})$, which appears to imply that \mathcal{T} is not a symmetry. And yet this cannot be because we established that \mathcal{T} was a physical symmetry from the outset, and the mathematical act of applying a unitary transformation shouldn't change this fact.

This apparent contradiction is resolved if we recognize that $\mathcal{T} \neq K$ in this new representation. Since the operation $\exp(i\mathbf{q}\cdot\mathbf{x})$ boosted our system by $-\mathbf{q}$, the proper action of time-reversal is to first boost into a representation in which it acts simply, apply K , then boost back. One can check that $\mathcal{T} = \exp(-i\mathbf{q}\cdot\mathbf{x})K\exp(i\mathbf{q}\cdot\mathbf{x}) = K\exp(2i\mathbf{q}\cdot\mathbf{x})$ does just the trick. A gauge transformation, such as the phase twist described, has the effect of bringing us into a physically equivalent but (possibly) mathematical distinct description of our system. Regardless of our choice of gauge, if we demand that \mathcal{T} be a symmetry of h , then there exists a representation of \mathcal{T} such that $h = \mathcal{T}^{-1}h\mathcal{T}$ regardless of the shape of h .

Consider now the following (bilayer) Hamiltonian,

$$H = \begin{pmatrix} h(\hat{\mathbf{p}}) & T(\mathbf{x}) \\ T(\mathbf{x})^* & h(\hat{\mathbf{p}} + \mathbf{q}_0) \end{pmatrix} \quad (\text{S1})$$

which describes a local tunneling between two identical layers. Note that as written, the tunneling appears to bring a particle from one layer into a boosted frame of an otherwise identical layer. Let us demand that \mathcal{T} be a symmetry of H . In order for H to be invariant under \mathcal{T} ,

$$T(\mathbf{x})^* e^{i(2\mathbf{q}_0)\cdot\mathbf{x}} = T(\mathbf{x}), \quad (\text{S2})$$

where the phase comes from the non-trivial action of \mathcal{T} in the boosted layer. Notice that Eqn S2 tells us the tunneling cannot be constant and preserve \mathcal{T} . The solution to Eqn S2 is a tunneling which is periodic under spatial shift reciprocal to $\mathbf{g}_1 = 2\mathbf{q}_0$. Which is to say that time-reversal symmetric tunneling between different Galilean frames generates a periodic lattice in at least one direction. If additional symmetries are present (e.g C_N rotations), then a lattice is generated which respects those symmetries (such as square for C_4). The action of any point-group operation g on H follows similarly to \mathcal{T} , i.e $\mathcal{U}g\mathcal{U}^*$ with \mathcal{U} defined in (5).

Any such emergent lattice is guaranteed to have an emergent sublattice degree of freedom. This is because we are free to apply a unitary transformation which moves us into a representation without the relative boost between the diagonal terms of Eqn S1, but where the information of the relative boost has been pushed onto the off diagonal,

$$H_f = \mathcal{U}^* H \mathcal{U} = \begin{pmatrix} h(\hat{\mathbf{p}}) & T(\mathbf{x})e^{-i\mathbf{q}_0\cdot\mathbf{x}} \\ T(\mathbf{x})^*e^{i\mathbf{q}_0\cdot\mathbf{x}} & h(\hat{\mathbf{p}}) \end{pmatrix}. \quad (\text{S3})$$

This is equivalent to a folding of the original zone, which changes the translational symmetry of the eigenstates, such that they become Bloch states of an enlarged unit cell.

2. Boosts by rotating a crystal

Let us start by defining a set of fixed ‘‘lab’’ coordinates, $\mathbf{x} \in \{n\mathbf{a}_1 + m\mathbf{a}_2 | (n, m) \in \mathbb{Z}^2\}$, which describes a set of discrete periodic sites. Now consider a single crystal plane with lattice coordinates $\mathbf{r}_\theta \in \{nR_\theta\mathbf{a}_1 + mR_\theta\mathbf{a}_2 | (n, m) \in \mathbb{Z}^2\}$, or equivalently $\mathbf{r}_\theta = R_\theta\mathbf{x}$, which implicitly defines the reciprocal lattice $\mathbf{G}_\theta \in \{nR_\theta\mathbf{G}_1 + mR_\theta\mathbf{G}_2 | (n, m) \in \mathbb{Z}^2\}$ via the relationship $e^{i\mathbf{G}_\theta\cdot\mathbf{r}_\theta} = 1$. We label the annihilation/creation operators for the tightly bound orbitals of this lattice $d(\mathbf{r}_\theta)/d^\dagger(\mathbf{r}_\theta)$. For our purposes, it is sufficient to consider one orbital per atomic cell, which corresponds to one band. Expanding $\hat{d}(\mathbf{r}_\theta)$ into crystal momenta

$$\hat{d}(\mathbf{r}_\theta) = \sum_{\mathbf{k}} e^{i(\mathbf{M}_\theta + \mathbf{k})\cdot\mathbf{r}_\theta} \hat{d}_{\mathbf{M}_\theta + \mathbf{k}} \equiv e^{i\mathbf{M}_\theta\cdot\mathbf{r}_\theta} \hat{\psi}(\mathbf{r}_\theta), \quad (\text{S4})$$

where $\mathbf{M}_\theta \equiv R_\theta \mathbf{M}$ is the crystal momenta corresponding to the rotated BZ corner (M -point). In doing this expansion, we implicitly chose a representation of the wavefunction $e^{i\mathbf{M}_\theta \cdot \mathbf{r}_\theta} = e^{i\mathbf{M} \cdot \mathbf{x}}$ which is an eigenstate of periodic shifts by $\mathbf{r}_\theta \rightarrow \mathbf{r}_\theta + R_\theta \mathbf{a}_j$. This is the natural representation of the crystal, in the sense that the periodicity of the wavefunction aligns with that of the physical crystal axis. We are not constrained to this representation, and can choose another, e.g

$$\hat{d}(\mathbf{r}_\theta) = \sum_{\mathbf{k}} e^{i(\mathbf{M}+\mathbf{k}) \cdot \mathbf{r}_\theta} \left(e^{i(\mathbf{M}_\theta - \mathbf{M}) \cdot \mathbf{r}_\theta} \hat{d}_{\mathbf{M}_\theta + \mathbf{k}} \right) \equiv e^{i\mathbf{M} \cdot \mathbf{r}_\theta} \hat{\Psi}(\mathbf{x}). \quad (\text{S5})$$

If we define $\hat{d}_{\mathbf{M}+\mathbf{k}}(\mathbf{x}) \equiv e^{i(\mathbf{M}_\theta - \mathbf{M}) \cdot \mathbf{r}_\theta} \hat{d}_{\mathbf{M}_\theta + \mathbf{k}}$, we would see this is equivalent to expanding $\hat{d}(\mathbf{r}_\theta)$ into a BZ aligned with the the lab axis (\mathbf{x}), and thus disaligned with the physical crystal axis (\mathbf{r}_θ). In this representation, the wavefunctions appear to be eigenstates of shifts by $\mathbf{r}_\theta \rightarrow \mathbf{r}_\theta + \mathbf{a}_j$; however, because \mathbf{M}_θ isn't the corner of this chosen zone, the annihilation operator necessarily picks up a spatial dependence in order to guarantee the proper transformation of physical symmetries. (See Ref [62] for an example of non-trivial point group operations in twisted bilayer graphene.)

In order to demonstrate this effect, it will be useful to define an operator (like momentum), and study how it transforms under symmetry in either representation. For this purpose, we construct a Bloch-periodic momentum operator,

$$\begin{aligned} \hat{\mathbf{p}}_B &= \sum_{\mathbf{G}_\theta} \int_{\mathbf{r}_\theta} \hat{d}^\dagger(\mathbf{r}_\theta) \left(-i \nabla_{\mathbf{r}_\theta} + \mathbf{G}_\theta \right) \hat{d}(\mathbf{r}_\theta) \\ &= \sum_{\mathbf{G}_\theta} \int_{\mathbf{r}_\theta} \hat{\psi}^\dagger(\mathbf{r}_\theta) \left(-i \nabla_{\mathbf{r}_\theta} + \mathbf{M}_\theta + \mathbf{G}_\theta \right) \hat{\psi}(\mathbf{r}_\theta), \end{aligned} \quad (\text{S6})$$

which is just the momentum operator projected onto Bloch states. (We employ the notation $\int_{\mathbf{x}} \equiv \int d^2\mathbf{x}$.) Notice that $\hat{\mathbf{p}}_B$ is defined modulo a reciprocal lattice vector aligned with the crystal axis (\mathbf{G}_θ), such that it is invariant under inserting the identity $e^{i\mathbf{G}_\theta \cdot \mathbf{r}_\theta} = 1$. The action of \mathcal{T} in this representation is the complex conjugate, which brings $\hat{\mathbf{p}}_B$ into

$$\mathcal{T}[\hat{\mathbf{p}}_B] = \sum_{\mathbf{G}_\theta} \int_{\mathbf{r}_\theta} \hat{\psi}^\dagger(\mathbf{r}_\theta) \left(+i \nabla_{\mathbf{r}_\theta} + \mathbf{M}_\theta + \mathbf{G}_\theta \right) \hat{\psi}(\mathbf{r}_\theta), \quad (\text{S7})$$

but because there exists a \mathbf{G}_θ such that $\mathbf{M}_\theta = \mathbf{G}_\theta - \mathbf{M}_\theta$, we can write

$$= \sum_{\mathbf{G}_\theta} \int_{\mathbf{r}_\theta} \hat{\psi}^\dagger(\mathbf{r}_\theta) \left(+i \nabla_{\mathbf{r}_\theta} - \mathbf{M}_\theta - \mathbf{G}_\theta \right) \hat{\psi}(\mathbf{r}_\theta) = -\hat{\mathbf{p}}_B. \quad (\text{S8})$$

This is the expected action of momentum under \mathcal{T} . In the other (Ψ) representation, this is not the case. Noting the identity $\mathbf{x} \cdot \nabla_{\mathbf{x}} = \mathbf{r}_\theta \cdot \nabla_{\mathbf{r}_\theta}$, we can write Eqn S6 as

$$\hat{\mathbf{p}}_B = \sum_{\mathbf{G}_\theta} \int_{\mathbf{x}} \hat{\Psi}^\dagger(\mathbf{x}) \left(-i R_\theta \nabla_{\mathbf{x}} + \mathbf{M} + \mathbf{G}_\theta \right) \hat{\Psi}(\mathbf{x}), \quad (\text{S9})$$

which is centered on \mathbf{M} and not \mathbf{M}_θ . Since \mathbf{M} is not connected to $-\mathbf{M}$ by some \mathbf{G}_θ , we cannot employ that strategy in guaranteeing the physical condition $\mathcal{T}[\hat{\mathbf{p}}_B] = -\hat{\mathbf{p}}_B$. The solution is that, in addition to complex conjugation, $\hat{\Psi}$ picks up a phase under \mathcal{T} :

$$\mathcal{T}[\hat{\psi}(\mathbf{r}_\theta)] = K \hat{\psi}(\mathbf{r}_\theta) \quad (\text{S10})$$

$$\mathcal{T}[\hat{\Psi}(\mathbf{x})] = K e^{i2\mathbf{M} \cdot \mathbf{r}_\theta} \hat{\Psi}(\mathbf{x}) = K e^{i2(\mathbf{M} - \mathbf{M}_\theta) \cdot \mathbf{r}_\theta} \hat{\Psi}(\mathbf{x}). \quad (\text{S11})$$

The quantity $(\mathbf{M} - \mathbf{M}_\theta) \cdot \mathbf{r}_\theta = \mathbf{M} \cdot (R_\theta \mathbf{x} - \mathbf{x})$ carries information about the displacement $\mathbf{u}_\theta \equiv R_\theta \mathbf{x} - \mathbf{x}$ of our rigidly-rotated layer from the lab frame [49].

Because rotating a crystal rotates the crystal BZ, this change of representation into a rotated frame of reference is equivalent to a boost for modes labelled by $\mathbf{k} \neq 0$, such as for $\mathbf{k} = \mathbf{M}$. Just as with \mathcal{T} , the choice of boosted frame has the effect of mutating point-group operations into space-group operations via the introduction of the phase factors. The effect of the boost is trivial in the case of a single layer, as we are always free to choose the natural representation of the crystal. But in the case of twisted bilayers, the relative rotation between the crystals is physical, the effect of which is preserved regardless of our choice of gauge.

To understand this explicitly, consider the case of twisted bilayers with relative displacement $\mathbf{u} = \mathbf{u}_{\theta/2} - \mathbf{u}_{-\theta/2} = R_{\theta/2}\mathbf{x} - R_{-\theta/2}\mathbf{x}$. We then write the Hamiltonian

$$\hat{H} = \int_{\mathbf{x}} \hat{\Psi}^\dagger(\mathbf{x}) \begin{pmatrix} h(-iR_{-\theta/2}\nabla_{\mathbf{x}} + \mathbf{M}) & T^*(\mathbf{x}) \\ T(\mathbf{x}) & h(-iR_{\theta/2}\nabla_{\mathbf{x}} + \mathbf{M}) \end{pmatrix} \hat{\Psi}(\mathbf{x}), \quad (\text{S12})$$

where $\hat{\Psi} = (\hat{\Psi}_1, \hat{\Psi}_2)^T$ defines our layer-spinor space. Notice that by applying the gauge $\hat{\Psi}_l \rightarrow e^{-i\mathbf{M}\cdot\mathbf{x}}\hat{\Psi}_l$, we can recenter the layer's momenta about $\mathbf{M} = (\pi/a, \pi/a)$, which is the corner of the BZ aligned with our common ‘‘unrotated’’ lab coordinates, producing

$$\hat{H} = \int_{\mathbf{x}} \hat{\Psi}^\dagger(\mathbf{x}) \begin{pmatrix} h(-iR_{-\theta/2}\nabla_{\mathbf{x}} + \mathbf{M} - \mathbf{M}_{-\theta/2}) & T^*(\mathbf{x}) \\ T(\mathbf{x}) & h(-iR_{\theta/2}\nabla_{\mathbf{x}} + \mathbf{M} - \mathbf{M}_{\theta/2}) \end{pmatrix} \hat{\Psi}(\mathbf{x}) = \int_{\mathbf{x}} \hat{\Psi}^\dagger \tilde{H} \hat{\Psi}. \quad (\text{S13})$$

In order to guarantee the local form of the tunneling, $T(\mathbf{x})$, it is necessary to constrain the superposition $\hat{\Psi}_l$ to be over those modes in the vicinity of $\mathbf{M}_{(2l-3)\theta/2}$, which for our purposes are the relevant modes (i.e near the Fermi level). This is because at long-wavelengths the relevant inter-layer tunnelings guarantee $T(\mathbf{x})$ to be a local function of the common coordinate \mathbf{x} .

Moving into the $\hat{\psi}(\mathbf{x}) = (\hat{\psi}_1(R_{-\theta/2}\mathbf{x}), \hat{\psi}_2(R_{\theta/2}\mathbf{x}))^T$ representation removes the boost

$$\hat{H} = \int_{\mathbf{x}} \hat{\psi}^\dagger(\mathbf{x}) \begin{pmatrix} h(-iR_{-\theta/2}\nabla_{\mathbf{x}}) & U(\mathbf{x}) \\ U(\mathbf{x}) & h(-iR_{\theta/2}\nabla_{\mathbf{x}}) \end{pmatrix} \hat{\psi}(\mathbf{x}) = \int_{\mathbf{x}} \hat{\psi}^\dagger H_f \hat{\psi}, \quad (\text{S14})$$

but pushes $e^{i(\mathbf{M}_{\theta/2} - \mathbf{M}_{-\theta/2})\cdot\mathbf{x}}$ onto the tunneling $U(\mathbf{x}) = e^{i(\mathbf{M}_{\theta/2} - \mathbf{M}_{-\theta/2})\cdot\mathbf{x}}T^*(\mathbf{x})$. The wavevector $\mathbf{q}_M = -\mathbf{M}_{\theta/2} + \mathbf{M}_{-\theta/2}$ is *not* a moiré reciprocal lattice vector, and has the effect of doubling the moiré cell. Thus we can recognize $\hat{\Psi}$ and $\hat{\psi}$ as corresponding to the ‘‘unfolded’’ and ‘‘folded’’ representations of the moiré translation symmetry. The folding transformation is the unitary

$$\mathcal{U}_\theta = \begin{pmatrix} e^{-i(\mathbf{M}_{\theta/2} - \mathbf{M})\cdot\mathbf{x}} & 0 \\ 0 & e^{-i(\mathbf{M}_{-\theta/2} - \mathbf{M})\cdot\mathbf{x}} \end{pmatrix}, \quad (\text{S15})$$

which acts like $\mathcal{U}_\theta\psi = \Psi$. Because the space and translation groups are decoupled in folded representation, it can be convenient to treat H_f as the ‘‘seed’’ Hamiltonian, from which its non-trivial representations can be generated. (Noting: $\tilde{H} = \mathcal{U}^*H_f\mathcal{U}$ and $T^*(\mathbf{x}) = e^{-i(\mathbf{M}_{\theta/2} - \mathbf{M}_{-\theta/2})\cdot\mathbf{x}}U(\mathbf{x})$.) Starting from H_f and successively applying \mathcal{U}_θ or \mathcal{U}_θ^* , we can generate an infinite number of physically equivalent representations. The conjugate representation $H = \mathcal{U}H_f\mathcal{U}^* = H^*$ can be generated by the reverse application of \mathcal{U}_θ , and can be understood as a freedom in the direction of unfolding. Written explicitly,

$$\hat{H} = \int_{\mathbf{x}} (\mathcal{U}_\theta^*\hat{\psi})^\dagger \begin{pmatrix} h(-iR_{-\theta/2}\nabla_{\mathbf{x}} - \mathbf{M} + \mathbf{M}_{-\theta/2}) & T(\mathbf{x}) \\ T^*(\mathbf{x}) & h(-iR_{\theta/2}\nabla_{\mathbf{x}} - \mathbf{M} + \mathbf{M}_{\theta/2}) \end{pmatrix} \mathcal{U}_\theta^*\hat{\psi} = \int_{\mathbf{x}} (\mathcal{U}_\theta^*\hat{\psi})^\dagger H \mathcal{U}_\theta^*\hat{\psi}. \quad (\text{S16})$$

This latter H representation is the one used in the main text (Fig 1). The choice is arbitrary, differing only in the internal form of \hat{H} and in the representation of the symmetry operations required to leave the Hamiltonian invariant.

3. Deriving the local field theories from microscopics

Let us begin by writing the microscopic tight-binding Hamiltonian for the inter-layer tunneling (see Ref [63] for a more general formulation),

$$H_{\text{micro}} = \sum_{\mathbf{x}\mathbf{x}'} \hat{d}_1^\dagger(R_{-\theta/2}\mathbf{x})t(R_{-\theta/2}\mathbf{x} - R_{\theta/2}\mathbf{x}')\hat{d}_2(R_{\theta/2}\mathbf{x}') + \text{h.c.}, \quad (\text{S17})$$

which we have written in the coordinate basis \mathbf{x} where both crystal layers appear rotated. The Fourier transform follows

$$= \sum_{\mathbf{x}\mathbf{x}'} \left(\sum_{\mathbf{k}} e^{-i\mathbf{k}\cdot(R_{-\theta/2}\mathbf{x})} \hat{d}_1^\dagger(\mathbf{k}) \right) \left(\int_{\mathbf{q}} \tilde{t}_{\mathbf{q}} e^{i\mathbf{q}\cdot(R_{-\theta/2}\mathbf{x} - R_{\theta/2}\mathbf{x}')} \right) \left(\sum_{\mathbf{k}'} e^{i\mathbf{k}'\cdot(R_{\theta/2}\mathbf{x}')} \hat{d}_2(\mathbf{k}') \right) + \text{h.c.}, \quad (\text{S18})$$

where we employ the shorthand $\int_{\mathbf{q}} \equiv \int_{\mathbf{q} \in \mathbb{R}^2} \frac{d^2 \mathbf{q}}{(2\pi)^2}$. Since the Brillouin zones of the layers are rotated, the operators in momentum space satisfy $\hat{d}_l(\mathbf{k} + \mathbf{G}_{(2l-3)\frac{\theta}{2}}) = \hat{d}_l(\mathbf{k})$. Note that the tunneling process does not respect the translation symmetry of either crystal, and therefore its tunneling vector \mathbf{q} can be any real vector. Continuing we have

$$= \int_{\mathbf{q}} \sum_{\mathbf{k}\mathbf{k}'} \tilde{t}_{\mathbf{q}} \hat{d}_1^\dagger(\mathbf{k}) \hat{d}_2(\mathbf{k}') \left(\sum_{\mathbf{x}} e^{i\mathbf{x} \cdot (R_{\theta/2}\mathbf{q} - R_{\theta/2}\mathbf{k})} \right) \left(\sum_{\mathbf{x}'} e^{-i\mathbf{x}' \cdot (R_{-\theta/2}\mathbf{q} - R_{-\theta/2}\mathbf{k}')} \right) + \text{h.c.} \quad (\text{S19})$$

the last two terms in parenthesis are delta functions mod \mathbf{G} ,

$$= \int_{\mathbf{q}} \sum_{\mathbf{k}\mathbf{k}'} \tilde{t}_{\mathbf{q}} \hat{d}_1^\dagger(\mathbf{k}) \hat{d}_2(\mathbf{k}') \sum_{\mathbf{G}\mathbf{G}'} \delta^2(R_{\theta/2}\mathbf{q} - R_{\theta/2}\mathbf{k} + \mathbf{G}) \delta^2(R_{-\theta/2}\mathbf{q} - R_{-\theta/2}\mathbf{k}' + \mathbf{G}') + \text{h.c.}, \quad (\text{S20})$$

where \mathbf{G} labels the unrotated reciprocal lattice, i.e $e^{i\mathbf{G} \cdot \mathbf{x}} = 1$. Note that, in order to reduce clutter, we have absorbed (and will continue to absorb) any (additional) normalization factors into the definition of $\tilde{t}_{\mathbf{q}}$. The product of delta functions sets the constraint

$$\mathbf{q} = \mathbf{k} - \mathbf{G}_{-\frac{\theta}{2}} = \mathbf{k}' - \mathbf{G}'_{\frac{\theta}{2}}. \quad (\text{S21})$$

Evaluating the delta functions allows us to eliminate \mathbf{q} and \mathbf{k}' ,

$$H_{\text{micro}} = \sum_{\mathbf{k}} \sum_{\mathbf{G}} \tilde{t}_{\mathbf{k} - \mathbf{G}_{-\frac{\theta}{2}}} \hat{d}_1^\dagger(\mathbf{k}) \sum_{\mathbf{G}'} \hat{d}_2(\mathbf{k} + \mathbf{G}'_{\frac{\theta}{2}} - \mathbf{G}_{-\frac{\theta}{2}}) + \text{h.c.} \quad (\text{S22})$$

Which says that the moiré tunneling process connects any pair of momenta $(\mathbf{k}, \mathbf{k} + \mathbf{G}'_{\frac{\theta}{2}} - \mathbf{G}_{-\frac{\theta}{2}})$ from the BZ's of our rotated crystals.

We are only interested in the physics near the Fermi level, which here means the band extrema at \mathbf{M} . In other words, we only need to keep processes involving $\mathbf{k} \pmod{\mathbf{G}}$ such that the single-layer dispersion at \mathbf{k} can be approximated by a quadratic $h_l(\mathbf{k}) \simeq \mu(\mathbf{k} - R_{(2l-3)\frac{\theta}{2}}\mathbf{M})^2$. Higher-energy tunnelings exist, but at best contribute a slight renormalization of the bands near Fermi. Therefore, the relevant moiré tunneling processes are those involving a hopping to $\mathbf{k} \simeq R_{-\theta/2}\mathbf{M}$ in layer 1, which we can get by shifting $\mathbf{k} = \mathbf{M}_{-\frac{\theta}{2}} + \delta\mathbf{k}$,

$$\simeq \sum_{\delta\mathbf{k}} \sum_{\mathbf{G}} \tilde{t}_{\delta\mathbf{k} + \mathbf{M}_{-\frac{\theta}{2}} - \mathbf{G}_{-\frac{\theta}{2}}} \hat{d}_1^\dagger(\delta\mathbf{k} + \mathbf{M}_{-\frac{\theta}{2}}) \sum_{\mathbf{G}'} \hat{d}_2(\delta\mathbf{k} + \mathbf{M}_{-\frac{\theta}{2}} + \mathbf{G}'_{\frac{\theta}{2}} - \mathbf{G}_{-\frac{\theta}{2}}) + \text{h.c.}, \quad (\text{S23})$$

and keeping only small $\delta\mathbf{k}$. For an infinitely large system, we can replace $\sum_{\mathbf{k}} \rightarrow \int_{\mathbf{k}}$. The function $\tilde{t}_{\delta\mathbf{k} + \mathbf{M}_{-\frac{\theta}{2}} - \mathbf{G}_{-\frac{\theta}{2}}}$ is analytic in $\delta\mathbf{k}$. We can therefore approximate $\tilde{t}_{\delta\mathbf{k} + \mathbf{M}_{-\frac{\theta}{2}} - \mathbf{G}_{-\frac{\theta}{2}}} \simeq \tilde{t}_{\mathbf{M}_{-\frac{\theta}{2}} - \mathbf{G}_{-\frac{\theta}{2}}}$ to leading order in powers of small $|\delta\mathbf{k}| \ll |\mathbf{G}_1|$,

$$\simeq \int_{\delta\mathbf{k}} \sum_{\mathbf{G}} \tilde{t}_{\mathbf{M}_{-\frac{\theta}{2}} - \mathbf{G}_{-\frac{\theta}{2}}} \hat{d}_1^\dagger(\delta\mathbf{k} + \mathbf{M}_{-\frac{\theta}{2}}) \sum_{\mathbf{G}'} \hat{d}_2(\delta\mathbf{k} + \mathbf{M}_{-\frac{\theta}{2}} + \mathbf{G}'_{\frac{\theta}{2}} - \mathbf{G}_{-\frac{\theta}{2}}) + \text{h.c.} \quad (\text{S24})$$

The latter step has the effect of guaranteeing our tunneling potential is local in real space. In the previous section we learned

$$\hat{d}_1(\delta\mathbf{k} + \mathbf{M}_{-\frac{\theta}{2}}) = \int_{\mathbf{x}} e^{i\mathbf{k} \cdot \mathbf{x}} \hat{\psi}_1(R_{-\theta/2}\mathbf{x}) \quad (\text{S25})$$

$$\hat{d}_2(\delta\mathbf{k} + \mathbf{M}_{-\frac{\theta}{2}} + \mathbf{G}'_{\frac{\theta}{2}} - \mathbf{G}_{-\frac{\theta}{2}}) = \int_{\mathbf{x}'} e^{i\mathbf{k} \cdot \mathbf{x}'} e^{i(\mathbf{M}_{-\frac{\theta}{2}} - \mathbf{M}_{\frac{\theta}{2}}) \cdot \mathbf{x}'} e^{i(\mathbf{G}'_{\frac{\theta}{2}} - \mathbf{G}_{-\frac{\theta}{2}}) \cdot \mathbf{x}'} \hat{\psi}_2(R_{\theta/2}\mathbf{x}'). \quad (\text{S26})$$

Plugging these into Eqn S24 reveals

$$H_{\text{micro}} \simeq \int_{\mathbf{x}} \hat{\psi}_1^\dagger(R_{-\theta/2}\mathbf{x}) \left(\sum_{\mathbf{G}\mathbf{G}'} \tilde{t}_{\mathbf{M}_{-\frac{\theta}{2}} - \mathbf{G}_{-\frac{\theta}{2}}} e^{i(\mathbf{M}_{-\frac{\theta}{2}} - \mathbf{M}_{\frac{\theta}{2}}) \cdot \mathbf{x}} e^{i(\mathbf{G}'_{\frac{\theta}{2}} - \mathbf{G}_{-\frac{\theta}{2}}) \cdot \mathbf{x}} \right) \hat{\psi}_2(R_{\theta/2}\mathbf{x}) \equiv H_{\text{continuum}}, \quad (\text{S27})$$

which is the continuum limit in the folded (ψ) representation. The unfolded (Ψ) representation is identical but without the factor $e^{i(\mathbf{M}_{-\frac{\theta}{2}} - \mathbf{M}_{\frac{\theta}{2}}) \cdot \mathbf{x}}$,

$$H_{\text{continuum}} = \int_{\mathbf{x}} \hat{\Psi}_1^\dagger(\mathbf{x}) \left(\sum_{\mathbf{G}\mathbf{G}'} \tilde{t}_{\mathbf{M}_{-\frac{\theta}{2}} - \mathbf{G}_{-\frac{\theta}{2}}} e^{i(\mathbf{G}'_{\frac{\theta}{2}} - \mathbf{G}_{-\frac{\theta}{2}}) \cdot \mathbf{x}} \right) \hat{\Psi}_2(\mathbf{x}) + \text{h.c.} \quad (\text{S28})$$

The term in parenthesis is a sum over local superlattice potentials, i.e

$$\sum_{\mathbf{G}\mathbf{G}'} \tilde{t}_{\mathbf{M}_{-\frac{\theta}{2}} - \mathbf{G}_{-\frac{\theta}{2}}} e^{i(\mathbf{G}'_{\frac{\theta}{2}} - \mathbf{G}_{-\frac{\theta}{2}}) \cdot \mathbf{x}} = T(\mathbf{x}) + \sum_{\mathbf{G}} \tilde{T}_{\mathbf{G}}(\mathbf{x}), \quad (\text{S29})$$

where

$$T(\mathbf{x}) = \sum_{\mathbf{G}} \tilde{t}_{\mathbf{M}_{-\frac{\theta}{2}} - \mathbf{G}_{-\frac{\theta}{2}}} e^{i(\mathbf{G}_{\frac{\theta}{2}} - \mathbf{G}_{-\frac{\theta}{2}}) \cdot \mathbf{x}} \quad (\text{S30})$$

$$\tilde{T}_{\mathbf{G}}(\mathbf{x}) = \sum_{\mathbf{G}' \neq \mathbf{G}} \tilde{t}_{\mathbf{M}_{-\frac{\theta}{2}} - \mathbf{G}_{-\frac{\theta}{2}}} e^{i(\mathbf{G}'_{\frac{\theta}{2}} - \mathbf{G}_{-\frac{\theta}{2}}) \cdot \mathbf{x}} \quad (\text{S31})$$

are respectively the intra ($\mathbf{G} = \mathbf{G}'$) and inter-zone ($\mathbf{G} \neq \mathbf{G}'$) tunneling potentials.

Note that the primitive moiré wavevectors are $\mathbf{g}_k = R_{\frac{\theta}{2}} \mathbf{G}_k - R_{-\frac{\theta}{2}} \mathbf{G}_k$ for $k = 1, 2$. Therefore the vector $\mathbf{g} = \mathbf{G}_{\frac{\theta}{2}} - \mathbf{G}_{-\frac{\theta}{2}}$, where $\mathbf{g} \in \{n\mathbf{g}_1 + m\mathbf{g}_2 | (n, m) \in \mathbb{Z}^2\}$, labels the emergent moiré reciprocal lattice. Thus we can recognize $T(\mathbf{x})$ as being the moiré-periodic tunneling derived from symmetry in the main text. For $\tilde{T}_{\mathbf{G}}(\mathbf{x})$ coming from the $\mathbf{G} \neq \mathbf{G}'$ terms, we can rewrite $\mathbf{G}'_{\frac{\theta}{2}} - \mathbf{G}_{-\frac{\theta}{2}} = \mathbf{G}_{\frac{\theta}{2}} - \mathbf{G}_{-\frac{\theta}{2}} + \mathbf{G}'_{\frac{\theta}{2}} - \mathbf{G}_{\frac{\theta}{2}} = \mathbf{g} + \mathbf{G}'_{\frac{\theta}{2}} - \mathbf{G}_{\frac{\theta}{2}}$. Thus

$$e^{i(\mathbf{G}'_{\frac{\theta}{2}} - \mathbf{G}_{-\frac{\theta}{2}}) \cdot \mathbf{x}} = e^{i\mathbf{g} \cdot \mathbf{x}} \times e^{i(\mathbf{G}'_{\frac{\theta}{2}} - \mathbf{G}_{\frac{\theta}{2}}) \cdot \mathbf{x}} \quad (\text{S32})$$

is a product over a moiré-periodic wave $e^{i\mathbf{g} \cdot \mathbf{x}}$ and a wave $e^{i(\mathbf{G}'_{\frac{\theta}{2}} - \mathbf{G}_{\frac{\theta}{2}}) \cdot \mathbf{x}}$ which varies rapidly at the *atomic* scale. Because these two wavevectors aren't guaranteed to be commensurate for arbitrary (or any) θ , the corresponding periodicity of the $\tilde{T}_{\mathbf{G}}(\mathbf{x})$ terms *isn't* guaranteed to be the moiré one. (More on this in the following subsections.) However, because the argument of $\hat{d}_2(\delta\mathbf{k} + \mathbf{M}_{-\frac{\theta}{2}} + \mathbf{G}'_{\frac{\theta}{2}} - \mathbf{G}_{-\frac{\theta}{2}})$ in Eqn S24 is far away from its band extrema at $R_{\theta/2}\mathbf{M}$, such inter-zone tunnelings are necessarily irrelevant near the Fermi level. The only relevant terms are those which contribute to $T(\mathbf{x})$, and only when $\theta \ll 1$.

4. Moiré periodicity isn't the commensurate one

If there exists an angle $\theta = \theta_c$ such that the atomic wavevector $R_{\theta/2}\mathbf{G}_1$ is a commensurate fraction of moiré wavevectors, i.e

$$R_{\theta/2}\mathbf{G}_1 = n\mathbf{g}_1 + m\mathbf{g}_2 \quad (\text{S33})$$

for integers n, m ; then that angle is a commensurate angle, at which translation is a good microscopic symmetry. Starting from the definition of $\mathbf{G}_1 = 2\pi l_a^{-1}(1, 0)$ & $\mathbf{G}_2 = 2\pi l_a^{-1}(0, 1)$, Eqn S33 tells us the following must be true:

$$\begin{pmatrix} \cos(\theta/2) \\ \sin(\theta/2) \end{pmatrix} = 2 \sin(\theta/2) \begin{pmatrix} m \\ n \end{pmatrix}. \quad (\text{S34})$$

However clearly, the bottom components implies the relationship $1 = 2n$, which cannot be satisfied for integer n . Therefore, no θ exists at which the emergent moiré translations are a microscopic symmetry.

This does not mean there is no commensurate θ_c , only that at θ_c the microscopic translation symmetry isn't the moiré one. Instead it is the *double* moiré cell which is microscopically commensurate at θ_c , which is to say that the *folded* moiré zone is commensurate with the atomic one, i.e

$$R_{\theta/2}\mathbf{G}_1 = n\mathbf{g}_{1,f} + m\mathbf{g}_{2,f}, \quad (\text{S35})$$

where the folded reciprocal vectors at $\mathbf{g}_{1,f} = \mathbf{q}_M$ and $\mathbf{g}_{2,f} = C_4\mathbf{q}_M$. Eqn S35 says

$$\begin{pmatrix} \cos(\theta/2) \\ \sin(\theta/2) \end{pmatrix} = \sin(\theta/2) \begin{pmatrix} n+m \\ n-m \end{pmatrix}, \quad (\text{S36})$$

which demands $n = m + 1$ and

$$\frac{\cos(\theta/2)}{\sin(\theta/2)} = 2m + 1. \quad (\text{S37})$$

The commensurate angles are those which satisfy $\theta_c = 2 \arccos(2m + 1)$ for integer m . We numerically checked this formula for θ_c against the one in Ref [22], and found them to be identical in the domain $m > 0$.

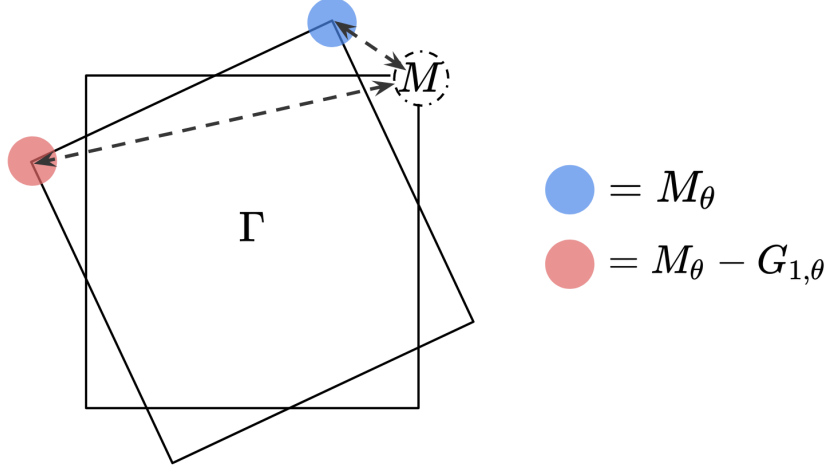


FIG. S1. Comparison of different inter-layer scattering contributions between rotated and unrotated layer M points: (1) intra-zone, and (2) inter-zone tunneling. The momentum of the inter-zone process is set by an atomic vector $G_{1,\theta}$, which is never commensurate with the intra-zone wavevector for any θ .

Appendix B: Tight-binding in the asymptotic limit of small θ

1. Notation

The following notations are used in the proceeding subsections: The superlattice period is denoted $l_S = l_a/\theta$. We write the ground state wavefunction of the harmonic oscillator $\psi_0(\mathbf{x})$, which is only used in Sec B 2 for calculating the projected Coulomb potential $U(r)$. The Mathieu wavefunctions are defined $\psi_\pm(\mathbf{x})$ with respect to the full solution to the Mathieu equations in Sec B 3, where \pm distinguishes the layer bonded/antibonded moiré sublattices. The Wannier functions corresponding to the Mathieu solutions are written $\omega_{\mathbf{R}}(\mathbf{x}, \pm)$.

In Sec B 5, we extend a lengthy calculation worked out in the supplement of Ref [53]. In order to stay consistent with their derivation, we introduced their notation in Sec B 5. This includes writing $\omega_{\mathbf{0}}(\mathbf{x}, -) = \psi(\tilde{x} - l_S)\psi(\tilde{y} - l_S)$, where ψ is the Wannier function for the ground state of the 1D Mathieu equation.

Any additional definitions are defined with respect to the above in their specific subsections.

2. Lattice of harmonic oscillators

To start, note that the definition of “layer-bonded” verse “layer-antibonded” is an arbitrary distinction. If we are given a layer-bonded state $|\text{top}\rangle + |\text{bottom}\rangle$, we can convert it to a layer-antibonded one by a redefinition of $|\text{bottom}\rangle' = -|\text{bottom}\rangle$.

The Hamiltonian for a layer-bonded sector follows from Eqn 7,

$$H_+(\mathbf{x}, \nabla) = -\mu\left(\partial_{\tilde{x}}^2 + \partial_{\tilde{y}}^2\right) + 2w_0\left(\cos(q_M\tilde{x}) + \cos(q_M\tilde{y})\right) = H_{\tilde{x}} + H_{\tilde{y}}. \quad (\text{S1})$$

Written in terms of coordinates axes which connect next-nearest neighbor sites, $\tilde{x} = (x + y)/\sqrt{2}$ & $\tilde{y} = (-x + y)/\sqrt{2}$, H_{1b} decouples into orthogonal 1D Hamiltonians. The expansion of the potential about its minima

$$H_{\tilde{x}} = -\mu\partial_{\tilde{x}}^2 - w_0q_M^2\tilde{x}^2 + \dots \quad (\text{S2})$$

can be truncated at quadratic order by taking $l_o/l_S \rightarrow 0$, where we can interpret $l_o = \sqrt{2}(\mu w_0^{-1})^{\frac{1}{4}}q_M^{-\frac{1}{2}}$ as measuring the charge spread of the ground state, i.e $\psi_0(\tilde{x}) \propto e^{-(\tilde{x}/l_o)^2}$. The 2D ground state follows from separation of variables

$$\psi_0(\tilde{x}, \tilde{y}) = \frac{\sqrt{2/\pi}}{l_o} \exp\left(-\frac{\tilde{x}^2 + \tilde{y}^2}{l_o^2}\right). \quad (\text{S3})$$

By comparison with the canonical form $H_x = -\hbar^2/(2m)\partial_x^2 + m\omega^2 x^2/2$, we have $\hbar^2/(2m) \equiv \mu$ and $m\omega^2/2 \equiv w_0 q_M^2$. The gap in this limit is the oscillator gap $E_{\text{gap}} = \hbar\omega = 4\sqrt{w_0}E_C$, where $E_C \equiv \mu q_M^2/4$. (The E_C notation is relevant for comparisons with Ref [53] in Sec B 5.)

Consider density-density interactions between sites connected by some arbitrary distance vector $\mathbf{d} = (d_x, d_y)$, and wavefunction normalization $N \equiv l_o^{-1}\sqrt{2/\pi}$:

$$(4\pi\epsilon/e^2)U(\mathbf{d}) = \frac{1}{2} \int_{\mathbf{r}\mathbf{r}'} \left(\psi_o(\mathbf{r} - \mathbf{d}) \right)^2 \frac{1}{|\mathbf{r} - \mathbf{r}'|} \left(\psi_o(\mathbf{r}') \right)^2 = N^4 \frac{1}{2} \int_{\mathbf{r}\mathbf{r}'} e^{-2l_o^{-2}(\mathbf{r}-\mathbf{d})^2} e^{-2l_o^{-2}\mathbf{r}'^2} \frac{1}{|\mathbf{r} - \mathbf{r}'|}. \quad (\text{S4})$$

Which decouples into center-of-mass (\mathbf{R}) and relative coordinate parts (ρ), via the map $\mathbf{r} = \mathbf{R} + \frac{1}{2}\rho$ & $\mathbf{r}' = \mathbf{R} - \frac{1}{2}\rho$,

$$\begin{aligned} &= N^4 \frac{1}{2} \int_{\mathbf{R}} \int_0^\infty d\rho \int_{-\pi}^\pi d\phi e^{-2l_o^{-2}(\mathbf{R} + \frac{1}{2}\rho - \mathbf{d})^2} e^{-2l_o^{-2}(\mathbf{R} - \frac{1}{2}\rho)^2} \\ &= \frac{N^4}{2} e^{-2l_o^{-2}d^2} \left(\int_0^\infty dR R e^{-4l_o^{-2}R^2} \int_{-\pi}^\pi d\theta e^{4l_o^{-2}\mathbf{d}\cdot\mathbf{R}} \right) \left(\int_0^\infty d\rho e^{-l_o^{-2}\rho^2} \int_{-\pi}^\pi d\phi e^{2l_o^{-2}\mathbf{d}\cdot\rho} \right) \\ &= \frac{N^4}{2} e^{-2l_o^{-2}d^2} \left(\frac{\pi}{4l_o^{-2}} e^{l_o^{-2}d^2} \right) \left(\frac{\pi^{3/2}}{\sqrt{l_o^{-2}}} e^{\frac{l_o^{-2}d^2}{2}} I_0\left(\frac{l_o^{-2}d^2}{2}\right) \right) \\ &= \frac{N^4 \pi^{5/2}}{8l_o^{-3}} e^{-\frac{l_o^{-2}d^2}{2}} I_0\left(\frac{l_o^{-2}d^2}{2}\right), \end{aligned} \quad (\text{S5})$$

where in going to the second-to-last line, we used the fact that

$$\int_0^\infty d\rho e^{-\alpha\rho^2} \int_{-\pi}^\pi d\phi e^{2(\beta_x \cos\phi + \beta_y \sin\phi)\rho} = \frac{\pi^{3/2}}{\sqrt{\alpha}} e^{\frac{\beta^2}{2\alpha}} I_0\left(\frac{\beta^2}{2\alpha}\right). \quad (\text{S6})$$

Or equivalently

$$I_0\left(\frac{\beta^2}{2\alpha}\right) = \frac{\sqrt{\alpha}}{\pi^{3/2}} e^{-\frac{\beta^2}{2\alpha}} \int_0^\infty d\rho e^{-\alpha\rho^2} \int_{-\pi}^\pi d\phi e^{2(\beta_x \cos\phi + \beta_y \sin\phi)\rho}, \quad (\text{S7})$$

is the zeroth modified Bessel function ($I_0(x) = J_0(ix)$), which satisfies the Bessel differential equation

$$x^2 \frac{d^2 I_0}{dx^2} + x \frac{dI_0}{dx} - x^2 I_0 = 0. \quad (\text{S8})$$

3. Mathieu equation and wavefunctions

Here we demonstrate that Eqn. 7 can be exactly solved using 1D Mathieu functions. Without loss of generality, we consider here the + sector (the degenerate solutions in "-" sector are obtained by $\mathbf{x} \rightarrow \mathbf{x} + \mathbf{R}_1$), for which the wavefunction satisfies:

$$-\mu \left(\partial_{\tilde{x}}^2 + \partial_{\tilde{y}}^2 \right) + 2w_0 \left(\cos(q_M \tilde{x}) + \cos(q_M \tilde{y}) \right) \psi_+(\tilde{x}, \tilde{y}) = E \psi_+(\tilde{x}, \tilde{y}),$$

where $q_M = \sqrt{2\pi}/l_a$ and \tilde{x}, \tilde{y} are oriented along $\mathbf{g}_1 + \mathbf{g}_2$ and $\mathbf{g}_1 - \mathbf{g}_2$, respectively. One notices that a solution can be found with variable separation ansatz $\psi_+(\tilde{x}, \tilde{y}) = X(\tilde{x})Y(\tilde{y})$, such that result satisfies:

$$E = E_X + E_Y, \quad (\text{S9})$$

$$-\mu \partial_{\tilde{x}}^2 X(\tilde{x}) + 2w_0 \cos(q_M \tilde{x}) X(\tilde{x}) = E_X X(\tilde{x}), \quad (\text{S10})$$

$$-\mu \partial_{\tilde{y}}^2 Y(\tilde{y}) + 2w_0 \cos(q_M \tilde{y}) Y(\tilde{y}) = E_Y Y(\tilde{y}). \quad (\text{S11})$$

The equations for $X(\tilde{x})$ and $Y(\tilde{y})$ can be reduced to the following dimensionless form:

$$\xi''(z) + [a - 2q \cos(2z)]\xi(z) = 0, \quad (\text{S12})$$

where $q = w_0/(\mu q_M^2/4) = \left(\frac{\theta^*}{\theta}\right)^2$ and $a = E_{X,Y}/(\mu q_M^2/4)$. The equation above is the Mathieu equation. The eigenenergies correspond to the lowest band are found from characteristic values $a_r(q)$, where $r \in (-1, 1)$ is the

Mathieu characteristic exponent corresponding to momentum in the Brillouin zone. Corresponding real symmetric eigenfunctions (which correspond to superpositions between k in $-k$) are $ce_r(z, q)$ - the periodic Mathieu functions, normalized to $\int_0^{2\pi} dz ce_r(z, q)^2 = \pi$.

The bandwidth $E^{max} - E^{min}$ is equal to $E_X^{max} - E_X^{min} + E_Y^{max} - E_Y^{min} = 2(\mu q_M^2/4)[a_1(1, q) - a_1(0, q)] = 2w_0(\theta/\theta^*)^2[a_1(1, q) - a_1(0, q)]$ leading to (8) of the main text using $W = 8t'$ in $V = 0$ case.

For the wavefunctions overlaps, Eqn. (9) of the main text, $\langle \psi_+^{\mathbf{k}=0} | \psi_-^{\mathbf{k}=0} \rangle$ one gets: $\langle \psi_+^{\mathbf{k}=0} | \psi_-^{\mathbf{k}=0} \rangle = \langle X^{\mathbf{k}=0} | X^{\mathbf{k}=0}(\tilde{x} + \mathbf{R}_1^{\tilde{x}}) \rangle \langle Y^{\mathbf{k}=0} | Y^{\mathbf{k}=0}(\tilde{y} + \mathbf{R}_1^{\tilde{y}}) \rangle$, where $\mathbf{R}_1^{\tilde{x}/\tilde{y}}$ is the component of \mathbf{R}_1 along \tilde{x}/\tilde{y} . The latter is expressed via the Mathieu functions as $(\int_0^\pi dx ce_0(x, q) ce_0(x + \pi/2, q))^2 / (\pi^2/4)$, where we used the π -periodicity of the $r = 0$ Mathieu functions.

4. Wannier orbitals and tight-binding formalism

We begin by demonstrating how the relevant Wannier orbitals are related to the basis states $|\mathbf{x}, l\rangle$ of the continuum Hamiltonian Eqn 6, where $l = 1, 2$ is the layer index. Note that this means we are choosing $|\mathbf{x}, l\rangle$ to be in the ‘‘folded’’ representation, such that $\hat{\Psi}_l(\mathbf{x})^\dagger |0\rangle = |\mathbf{x}, l\rangle$. Since we know that Eqn 6 is diagonal in the layer-bonding/antibonding basis, it will be more convenient for us to start by first rotating into this basis, defining

$$|\mathbf{x}, \pm\rangle = \frac{|\mathbf{x}, 1\rangle \pm |\mathbf{x}, 2\rangle}{\sqrt{2}}, \quad (\text{S13})$$

which we will write as $|\mathbf{x}, \lambda\rangle$ where $\lambda = \pm$ is the index. The Fourier transform of $|\mathbf{x}, \lambda\rangle$ are plane waves labelled by momenta \mathbf{p} , which we integrate over in the limit of an infinitely large system,

$$\langle \mathbf{x}, \lambda | = \int_{\mathbf{p}} e^{i\mathbf{x}\cdot\mathbf{p}} \langle \mathbf{p}, \lambda |. \quad (\text{S14})$$

Note that H_f (Eqn 6) is a folded representation of H (Eqn 1), which is periodic under an enlarged cell defined by basis vectors $\mathbf{R}_{f,1} = (\mathbf{R}_1 + \mathbf{R}_2)/2$ and $C_4\mathbf{R}_{f,2}$. Because of this, we choose to relabel our continuum momenta $\mathbf{p} = \mathbf{k}_f + \mathbf{g}_f$, where \mathbf{g}_f spans the discrete set of folded reciprocal lattice vectors, and \mathbf{k}_f is a continuous variable which lies within the first folded zone. With this choice Eqn S14 becomes

$$= \int_{\mathbf{k}_f} \sum_{\mathbf{g}_f} e^{i\mathbf{x}\cdot(\mathbf{k}_f + \mathbf{g}_f)} \langle \mathbf{k}_f + \mathbf{g}_f, \lambda |. \quad (\text{S15})$$

Translational invariance means that \mathbf{k}_f is a conserved quantity, which has the consequence that the matrix structure of H_f is block diagonal in the $\langle \mathbf{k}_f + \mathbf{g}_f, \lambda |$ basis, where each independent block is labelled by \mathbf{k} . Additionally, without additional perturbations (V or (B_x, B_y)), H_f is diagonal in the λ basis, such that the Bloch states are layer-bonded/antibonded eigenstates. Therefore each value of (\mathbf{k}_f, λ) has a unitary transformation $u_{\mathbf{g}_f, \xi}(\mathbf{k}_f, \lambda)$ which diagonalizes the blocks (the u here should not to be confused with the displacement defined below equation (S11) in Appendix A), i.e $\langle \mathbf{k}_f + \mathbf{g}_f, \lambda | = \sum_{\xi} u_{\mathbf{g}_f, \xi}(\mathbf{k}_f, \lambda) \langle \mathbf{k}_f, \xi, \lambda |$, where index ξ labels the discrete set of energy bands at each value of (\mathbf{k}_f, λ) , and \mathbf{g}_f indexes the infinitely-many continuum plane waves with flavour λ . Rotating into the band basis allows us to reorganize Eqn S16 into the form

$$= \sum_{\xi} \int_{\mathbf{k}_f} e^{i\mathbf{x}\cdot\mathbf{k}_f} \left(\sum_{\mathbf{g}_f} e^{i\mathbf{x}\cdot\mathbf{g}_f} u_{\mathbf{g}_f, \xi}(\mathbf{k}_f, \lambda) \right) \langle \mathbf{k}_f, \xi, \lambda | \equiv \sum_{\xi} \int_{\mathbf{k}_f} e^{i\mathbf{x}\cdot\mathbf{k}_f} u_{\xi, \mathbf{k}_f}(\mathbf{x}, \lambda) \langle \mathbf{k}_f, \xi, \lambda |. \quad (\text{S16})$$

One may recognize $u_{\xi, \mathbf{k}_f}(\mathbf{x}, \lambda)$ as being the periodic part of the Bloch function, satisfying $u_{\xi, \mathbf{k}_f}(\mathbf{x} + \mathbf{R}_f, \lambda) = u_{\xi, \mathbf{k}_f}(\mathbf{x}, \lambda)$ for any $\mathbf{R}_f \in \{n\mathbf{R}_{f,1} + m\mathbf{R}_{f,2} | (n, m) \in \mathbb{Z}^2\}$. The full Bloch wavefunction is therefore $\Psi_{\xi, \mathbf{k}_f}(\mathbf{x}, \lambda) = e^{i\mathbf{x}\cdot\mathbf{k}_f} u_{\xi, \mathbf{k}_f}(\mathbf{x}, \lambda)$.

For our purposes, the relevant bands are those near the Fermi level, of which there are two in the folded representation. We therefore fix $\xi = 1$, which we choose to label the moire band in either λ sector. Since the index is irrelevant from here out, we will drop it, with the understanding that λ now distinguishes the two degenerate low-energy bands.

Because we have only a single band per λ , their Fourier transformation are localized Wannier orbitals, i.e $|\mathbf{k}_f, \lambda\rangle = \sum_{\mathbf{R}_f} e^{i\mathbf{R}_f \cdot \mathbf{k}_f} |\mathbf{R}_f, \lambda\rangle$. Thus Eqn S16 becomes

$$\langle \mathbf{x}, \lambda | = \sum_{\mathbf{R}_f} \left(\int_{\mathbf{k}_f} e^{-i\mathbf{R}_f \cdot \mathbf{k}_f} \Psi_{\mathbf{k}_f}(\mathbf{x}, \lambda) \right) \langle \mathbf{R}_f, \lambda | = \sum_{\mathbf{R}_f} \omega_{\mathbf{R}_f}(\mathbf{x}, \lambda) \langle \mathbf{R}_f, \lambda |. \quad (\text{S17})$$

or equivalently

$$\omega_{\mathbf{R}_f}(\mathbf{x}, \lambda) = \sum_{\mathbf{k}_f} e^{-i\mathbf{R}_f \cdot \mathbf{k}_f} \Psi_{\mathbf{k}_f}(\mathbf{x}, \lambda). \quad (\text{S18})$$

These Wannier functions $\omega_{\mathbf{R}_f}(\mathbf{x}, \lambda)$ are the Fourier transform of the ground states of the 2D Mathieu equations, the densities of which are centered at \mathbf{R}_f (or $\mathbf{R}_f + \mathbf{R}_1$) for $\lambda = +1$ (-1). Thus we write $\omega_{\mathbf{R}_f}(\mathbf{x}) \equiv \omega_{\mathbf{R}_f}(\mathbf{x}, +)$ and $\omega_{\mathbf{R}_f + \mathbf{R}_1}(\mathbf{x}) = \omega_{\mathbf{R}_f}(\mathbf{x} - \mathbf{R}_1) \equiv \omega_{\mathbf{R}_f}(\mathbf{x}, -)$, where again $\mathbf{R}_1 = (\mathbf{R}_{f,1} - \mathbf{R}_{f,2})/2$ is the moiré lattice vector.

What are the Wannier functions in the unfolded representation? The Wannier functions in the folded/unfolded representations cannot be the same. This is because for fixed \mathbf{R}_f , the pair of Wannier functions for different λ correspond to different sublattices, and thus may have a finite overlap. However, in the unfolded representation, the pair of localized sublattices is replaced with a single set of orthogonal Wannier functions, which necessarily have vanishing overlaps. To construct the unfolded set of Wannier functions, we can take advantage of the boost Eqn 5 to shift one layer band relative from the other by momentum \mathbf{q}_M . For our purposes here, we will choose to use a modified version of Eqn 5, which fixes the first layer at $\mathbf{k} = 0$ while boosting the second. (The choice amounts to an arbitrary shift in the definition of the moiré BZ boundary.)

$$\begin{pmatrix} \langle \mathbf{x}, 1 \rangle' \\ \langle \mathbf{x}, 2 \rangle' \end{pmatrix} = \begin{pmatrix} 1 & 0 \\ 0 & e^{i\mathbf{x} \cdot \mathbf{q}_M} \end{pmatrix} \begin{pmatrix} \langle \mathbf{x}, 1 \rangle \\ \langle \mathbf{x}, 2 \rangle \end{pmatrix}. \quad (\text{S19})$$

Which according to Eqn S13 means,

$$\langle \mathbf{x}, \lambda \rangle' = \frac{1}{\sqrt{2}} \left(\langle \mathbf{x}, 1 \rangle + \lambda e^{-i\mathbf{x} \cdot \mathbf{q}_M} \langle \mathbf{x}, 2 \rangle \right). \quad (\text{S20})$$

Inverting Eqn S13 for $\langle \mathbf{x}, l \rangle$ and plugging back into the above produces

$$= \frac{1}{2} \sum_{\mathbf{R}_f} \left(\omega_{\mathbf{R}_f}(\mathbf{x}, +) (1 + \lambda e^{-i\mathbf{x} \cdot \mathbf{q}_M}) \langle \mathbf{R}_f, + | + \omega_{\mathbf{R}_f}(\mathbf{x}, -) (1 - \lambda e^{-i\mathbf{x} \cdot \mathbf{q}_M}) \langle \mathbf{R}_f, - | \right). \quad (\text{S21})$$

Note that we are free to relabel $\langle \mathbf{R}_f | \equiv \langle \mathbf{R}_f, + |$ & $\langle \mathbf{R}_f + \mathbf{R}_1 | \equiv \langle \mathbf{R}_f, - |$,

$$= \frac{1}{2} \sum_{\mathbf{R}_f} \left(\omega_{\mathbf{R}_f}(\mathbf{x}) (1 + \lambda e^{-i\mathbf{x} \cdot \mathbf{q}_M}) \langle \mathbf{R}_f | + \omega_{\mathbf{R}_f + \mathbf{R}_1}(\mathbf{x}) (1 - \lambda e^{-i\mathbf{x} \cdot \mathbf{q}_M}) \langle \mathbf{R}_f + \mathbf{R}_1 | \right), \quad (\text{S22})$$

and using the fact that $e^{i\mathbf{q}_M \cdot \mathbf{R}_{f,1}} = +1$ & $e^{i\mathbf{q}_M \cdot \mathbf{R}_1} = -1$,

$$= \frac{1}{2} \sum_{\mathbf{R}} \omega_{\mathbf{R}}(\mathbf{x}) (1 + \lambda e^{-i(\mathbf{x} - \mathbf{R}) \cdot \mathbf{q}_M}) \langle \mathbf{R} |, \quad (\text{S23})$$

taking note that the sum now runs over the moiré lattice sites (i.e \mathbf{R} w/o the subscript f). It then follows that the unfolded Wannier functions are

$$\tilde{\omega}_{\mathbf{R}}(\mathbf{x}, \lambda) = \frac{1 + \lambda e^{-i(\mathbf{x} - \mathbf{R}) \cdot \mathbf{q}_M}}{2} \omega_{\mathbf{R}}(\mathbf{x}). \quad (\text{S24})$$

Unlike the folded set of Wannier functions $\omega_{\mathbf{R}}(\mathbf{x})$, the unfolded Wannier functions are two-component vectors $\tilde{\omega}_{\mathbf{R}}(\mathbf{x}) = (\tilde{\omega}_{\mathbf{R}}(\mathbf{x}, +), \tilde{\omega}_{\mathbf{R}}(\mathbf{x}, -))^T$ in the bonded/antibonded space. Thus we can see that the Wannier function peaked at $\mathbf{x} = \mathbf{0}$, i.e $\tilde{\omega}_{\mathbf{0}}(\mathbf{x})$, is entirely bonding at its center $\mathbf{x} = \mathbf{0}$, and becoming antibonding at $\mathbf{x} = \mathbf{R}_1$. Further, one can check that the unfolded set is orthogonal between different \mathbf{R} & \mathbf{R}' , either because: (i) \mathbf{R} & \mathbf{R}' lie on the same folded sublattice, where $\omega_{\mathbf{R}}(\mathbf{x})$ are guaranteed orthogonal by construction; or (ii) \mathbf{R} & \mathbf{R}' are on different sublattices, but where $\tilde{\omega}_{\mathbf{R}}(\mathbf{x})^\dagger \tilde{\omega}_{\mathbf{R}'}(\mathbf{x})$ vanishes because of the phase. Despite this subtle distinction between the folded/unfolded sets of Wannier functions, their densities are identically: $\tilde{\omega}_{\mathbf{R}}(\mathbf{x})^\dagger \tilde{\omega}_{\mathbf{R}}(\mathbf{x}) = |\omega_{\mathbf{R}}(\mathbf{x})|^2$.

a. Hoppings: t, t' , t_x, t_y

We start by writing the Hamiltonian in the folded representation,

$$H = \sum_{\lambda\lambda'} \int_{\mathbf{x}} |\mathbf{x}, \lambda\rangle \begin{pmatrix} h(-i\nabla_{\mathbf{x}}) + U(\mathbf{x}) & \Delta h \\ \Delta h & h(-i\nabla_{\mathbf{x}}) - U(\mathbf{x}) \end{pmatrix}_{\lambda\lambda'} \langle \mathbf{x}, \lambda' |, \quad (\text{S25})$$

which is diagonal in the bonding-antibonding basis modulo perturbations $\Delta h \equiv (-V - 2\mu\mathbf{A} \cdot i\nabla)$. The hoppings within the tight-binding formalism are the projection of the Hamiltonian onto the localized Wannier functions,

$$\langle \mathbf{R}_f, \lambda | H | \mathbf{R}'_f, \lambda' \rangle = \int_{\mathbf{x}} \langle \mathbf{R} | \mathbf{x}, \lambda \rangle \begin{pmatrix} h(-i\nabla_{\mathbf{x}}) + U(\mathbf{x}) & \Delta h \\ \Delta h & h(-i\nabla_{\mathbf{x}}) - U(\mathbf{x}) \end{pmatrix}_{\lambda\lambda'} \langle \mathbf{x}, \lambda' | \mathbf{R}' \rangle, \quad (\text{S26})$$

where $\langle \mathbf{x}, \lambda' | \mathbf{R}'_f, \lambda' \rangle = \omega_{\mathbf{R}'_f}(\mathbf{x}, \lambda')$ follows from Eqn S17. (Remember that the difference between $\langle \mathbf{R} |$ and $\langle \mathbf{R}_f, \lambda |$ is just a relabelling, i.e $\langle \mathbf{R}_f, \lambda | \equiv \langle \mathbf{R}_f + \frac{1}{2}(1 - \lambda)\mathbf{R}_1 |$.) Thus we have

$$t' = \int_{\mathbf{x}} \omega_{\mathbf{R}_{f,1}}(\mathbf{x}, +) \left(h(-i\nabla_{\mathbf{x}}) + U(\mathbf{x}) \right) \omega_{\mathbf{0}}(\mathbf{x}, +) \quad (\text{S27})$$

and

$$t_x = \int_{\mathbf{x}} \omega_{\mathbf{0}}(\mathbf{x}, -) \Delta h \omega_{\mathbf{0}}(\mathbf{x}, +). \quad (\text{S28})$$

The real part of $t_x = t_x^r + it_x^i$,

$$t_x^r = -V \int_{\mathbf{x}} \omega_{\mathbf{0}}(\mathbf{x}, -) \omega_{\mathbf{0}}(\mathbf{x}, +) \quad (\text{S29})$$

comes from the application of V , which does not break C_4 such that $t_x^r = t_y^r$. Its imaginary part is generated by in-plane field,

$$t_x^i = -2\mu \int_{\mathbf{x}} \omega_{\mathbf{0}}(\mathbf{x}, -) (\mathbf{A} \cdot \nabla) \omega_{\mathbf{0}}(\mathbf{x}, +). \quad (\text{S30})$$

As demonstrated by Eqn S1, the 2D Mathieu equations decouple into 1D problems such that we can write $\omega_{\mathbf{0}}(\mathbf{x}, +) = \psi(\tilde{x})\psi(\tilde{y})$ and $\omega_{\mathbf{0}}(\mathbf{x}, -) = \psi(\tilde{x} - l_S)\psi(\tilde{y} - l_S)$, where ψ is the Wannier function for the ground state of the 1D Mathieu equation. Plugging this back into the formula

$$t_x^i = -2\mu \int_{\mathbf{x}} \psi(\tilde{x} - l_S)\psi(\tilde{y} - l_S) (A_{\tilde{x}}\partial_{\tilde{x}} + A_{\tilde{y}}\partial_{\tilde{y}}) \psi(\tilde{x})\psi(\tilde{y}) \quad (\text{S31})$$

$$= -2\mu A_{\tilde{x}} \left(\int_{\tilde{x}} \psi(\tilde{x} - l_S) \partial_{\tilde{x}} \psi(\tilde{x}) \right) \left(\int_{\tilde{y}} \psi(\tilde{y} - l_S) \psi(\tilde{y}) \right) - 2\mu A_{\tilde{y}} \left(\int_{\tilde{x}} \psi(\tilde{x} - l_S) \psi(\tilde{x}) \right) \left(\int_{\tilde{y}} \psi(\tilde{y} - l_S) \partial_{\tilde{y}} \psi(\tilde{y}) \right) \quad (\text{S32})$$

The direct overlaps of the 1D Wannier functions are dimensionless, but the overlaps of the gradient carry the dimensions of the gradient. We therefore non-dimensionalize by defining $\varphi \equiv q_M \tilde{x}$, where $\partial_{\tilde{x}} = q_M \partial_{\varphi}$, giving

$$= -2\mu A_{\tilde{x}} q_M \left(\int_{\varphi} \psi(\varphi - \pi) \partial_{\varphi} \psi(\varphi) \right) \left(\int_{\varphi'} \psi(\varphi' - \pi) \psi(\varphi') \right) - 2\mu A_{\tilde{y}} q_M \left(\int_{\varphi} \psi(\varphi - \pi) \psi(\varphi) \right) \left(\int_{\varphi'} \psi(\varphi' - \pi) \partial_{\varphi'} \psi(\varphi') \right) \quad (\text{S33})$$

$$= -2\mu (A_{\tilde{x}} + A_{\tilde{y}}) q_M \left(\int_{\varphi} \psi(\varphi - \pi) \partial_{\varphi} \psi(\varphi) \right) \left(\int_{\varphi'} \psi(\varphi' - \pi) \psi(\varphi') \right) \quad (\text{S34})$$

$$= -2\mu (A_{\tilde{x}} + A_{\tilde{y}}) q_M \mathcal{O}_0 \mathcal{O}_1, \quad (\text{S35})$$

where $\mathcal{O}_0 \equiv \int_{\varphi} \psi(\varphi - \pi) \psi(\varphi)$ and $\mathcal{O}_1 \equiv \int_{\varphi} \psi(\varphi - \pi) \partial_{\varphi} \psi(\varphi)$ are worked out in the next section. Now similarly,

$$t_y^i = -2\mu \int_{\mathbf{x}} \psi(\tilde{x} - l_S) \psi(\tilde{y} + l_S) (A_{\tilde{x}}\partial_{\tilde{x}} + A_{\tilde{y}}\partial_{\tilde{y}}) \psi(\tilde{x})\psi(\tilde{y}). \quad (\text{S36})$$

Using the fact that $\psi(\varphi) = \psi(-\varphi)$, we have $\int_{\varphi} \psi(\varphi + \pi) \partial_{\varphi} \psi(\varphi) = -\int_{\varphi} \psi(\varphi - \pi) \partial_{\varphi} \psi(\varphi)$, which we can use to get t_y^i .

Together,

$$t_x^i = -2\mu (A_{\tilde{x}} + A_{\tilde{y}}) q_M \mathcal{O}_0 \mathcal{O}_1 \quad (\text{S37})$$

$$t_y^i = -2\mu (A_{\tilde{x}} - A_{\tilde{y}}) q_M \mathcal{O}_0 \mathcal{O}_1. \quad (\text{S38})$$

Noting that in our original coordinates: $A_{\tilde{x}} + A_{\tilde{y}} = \sqrt{2}A_x$ and $A_{\tilde{x}} - A_{\tilde{y}} = \sqrt{2}A_y$.

5. WKB derivation of the overlaps

Because of the simplicity afforded by the folded representation, we were able to find analytical forms for our hoppings in the limit of flat isolated bands. Naively, one might try to calculate t & t' analytically using a linear combination of atomic orbitals (LCAO), where the atomic orbitals are taken to be the Gaussian wavefunctions of the 2D harmonic oscillator, which is the correct wavefunction in the atomic (i.e $\theta \rightarrow 0$) limit of Eqn 7. While quantities which depend only on densities – such as E_{gap} – can be derived from the harmonic oscillator, tunnelings which depend on the tails of the Wannier functions cannot [54]. This is because the wavefunction inside the potential barrier (i.e the classically forbidden region), where the overlap between neighboring sites is highest, is non-Gaussian. As was demonstrated for 1D [54], the asymptotic solutions to the Mathieu equations [54], as well as semi-classical solutions which account for the classical turning points [53, 54], capture the correct form of the hopping.

Because Eqn S1 decouples into two 1D Mathieu equations along orthogonal lines connecting next-to-nearest neighbor moiré sites, we were able to directly exploit the 1D solution [54] when writing t' (Eqn 8). However, exact 1D Mathieu solutions cannot be used to calculate t (Eqn 9). For this we calculate the semi-classical approximation to the wavefunction in the overlapping region, which follows from the derivation worked out in Appendix B in Ref [53] (where they worked out the semi-classical approximation of what is our t').

To keep consistent with the notation in [53], we'll write $E_C = \mu q_M^2/4$, $E_J = 2w_0$, and $\varphi \equiv q_M \tilde{x}$. Using this notation, the semi-classical momentum is

$$p(\varphi) = \frac{1}{\sqrt{4E_C}} \sqrt{V(\varphi) - E} = \frac{1}{\sqrt{4E_C}} \sqrt{-E + E_J(1 + \cos(\varphi))} \quad (\text{S39})$$

in the region $|\varphi| < \pi$. (Using $V(\varphi) = -E_J(1 + \cos \varphi)$ in line with Ref [53].) In the classically allowed region, $|\varphi| < a$ the ground state is the ground state of the Harmonic oscillator with energy $E = E_{\text{gap}}/2 - 2E_J = \sqrt{2E_J E_C} - 2E_J$; and where $a = \arccos(1 - \sqrt{2E_C/E_J})$, which is approximately $a \simeq 0$ in the asymptotic (small twist angle) limit $\sqrt{E_C/E_J} \rightarrow 0$. The semi-classical approximation in the region $a < \varphi < \pi$ has the form

$$\psi(\varphi) \simeq \frac{C_0}{2\sqrt{p(\varphi)}} \exp\left(-\int_a^\varphi d\varphi' p(\varphi')\right). \quad (\text{S40})$$

Note that $p(\varphi)$ can be rewritten as the sum of the following integrals,

$$\int_a^\varphi d\varphi' p(\varphi') = \int_a^\pi d\varphi' p(\varphi') - \int_{\pi/2}^\pi d\varphi' p(\varphi') - \int_\varphi^{\pi/2} d\varphi' p(\varphi'). \quad (\text{S41})$$

The solution to the first integral is in Ref [53] – see B14. In the limit $\sqrt{E_C/E_J} \rightarrow 0$, it becomes

$$\int_a^\pi d\varphi' p(\varphi') \simeq \sqrt{\frac{2E_J}{E_C}} \left(1 - \frac{1}{2} \sqrt{\frac{E_C}{2E_J}} \log \left[4 \left(\frac{2E_J}{E_C}\right)^{1/4}\right] - \frac{1}{4} \sqrt{\frac{E_C}{2E_J}}\right). \quad (\text{S42})$$

The second integral has the exact form

$$\int_{\pi/2}^\pi d\varphi' p(\varphi') = \sqrt{\frac{E_J}{4E_C}} \left(2 + \sqrt{2} \sqrt{\frac{E_C}{2E_J}} \log \left(\tan\left(\frac{\pi}{8}\right)\right)\right). \quad (\text{S43})$$

This leaves the third integral, which carries the φ dependence:

$$\begin{aligned} \int_\varphi^{\pi/2} d\varphi' p(\varphi') &= \sqrt{\frac{E_J}{4E_C}} \int_\varphi^{\pi/2} d\varphi' \sqrt{1 - \sqrt{\frac{2E_C}{E_J}} - \cos \varphi'} \\ &= \sqrt{\frac{E_J}{4E_C}} \int_\varphi^{\pi/2} d\varphi' \left(\sqrt{1 - \cos \varphi'} - \frac{1}{2} \sqrt{\frac{2E_C/E_J}{1 - \cos \varphi'}}\right) + \mathcal{O}\left(\sqrt{\frac{E_C}{E_J}}\right). \end{aligned} \quad (\text{S44})$$

The higher order corrections are irrelevant in the asymptotic limit. Dropping these and the remaining integral gives

$$= \sqrt{\frac{E_J}{4E_C}} \left(\frac{2}{3} \left(1 - \left(1 + \frac{\pi}{2} - \varphi \right)^{3/2} \right) - \sqrt{\frac{2E_C}{E_J}} \left(1 - \sqrt{1 + \frac{\pi}{2} - \varphi} \right) \right). \quad (\text{S45})$$

We keep the relevant contributions and now have

$$\psi(\varphi) \simeq \frac{C_0 e^{\frac{1}{4}} \sqrt{\tan(\pi/8)}}{\sqrt{p(\varphi)}} \left(\frac{E_C}{2E_J} \right)^{-\frac{1}{8}} e^{-\sqrt{\frac{2E_J}{E_C}} \left(1 - \frac{1}{\sqrt{2}} \right)} e^{-\frac{1}{3\sqrt{2}} \sqrt{\frac{2E_J}{E_C}} \left(-1 + \left(1 + \frac{\pi}{2} - \varphi \right)^{3/2} \right)} e^{-\frac{1}{\sqrt{2}} \left(1 - \sqrt{1 + \frac{\pi}{2} - \varphi} \right)}. \quad (\text{S46})$$

a. *Overlap \mathcal{O}_0*

The nearest-neighbor tunneling t depends on the overlap,

$$\begin{aligned} \int d\varphi \psi(\varphi) \psi(\pi - \varphi) &= \left(\frac{C_0 e^{\frac{1}{4}} \sqrt{\tan(\pi/8)}}{e^{\sqrt{\frac{2E_J}{E_C}} \left(1 - \frac{1}{\sqrt{2}} \right)}} \right)^2 \left(\frac{E_C}{2E_J} \right)^{-\frac{1}{4}} \\ &\times \int d\varphi \frac{e^{-\frac{1}{3\sqrt{2}} \sqrt{\frac{2E_J}{E_C}} \left(-2 + \left(1 + \frac{\pi}{2} - \varphi \right)^{3/2} + \left(1 - \frac{\pi}{2} + \varphi \right)^{3/2} \right)} e^{\frac{1}{\sqrt{2}} \left(-2 + \sqrt{1 + \frac{\pi}{2} - \varphi} + \sqrt{1 - \frac{\pi}{2} + \varphi} \right)}}{\sqrt{p(\varphi) p(\pi - \varphi)}} \end{aligned} \quad (\text{S47})$$

The peak of the integrand is at $\varphi = \pi/2$, so we change variables $z \equiv (\frac{\pi}{2} - \varphi)$ and expand the argument of the first exponential about $z = 0$,

$$= \left(\frac{C_0 e^{\frac{1}{4}} \sqrt{\tan(\pi/8)}}{e^{\sqrt{\frac{2E_J}{E_C}} \left(1 - \frac{1}{\sqrt{2}} \right)}} \right)^2 \left(\frac{E_C}{2E_J} \right)^{-\frac{1}{4}} \int dz \frac{e^{-\frac{1}{3} \sqrt{\frac{E_J}{E_C}} \left(\frac{3}{4} z^2 + \mathcal{O}(z^4) \right)} e^{\frac{1}{\sqrt{2}} \left(-2 + \sqrt{1+z} + \sqrt{1-z} \right)}}{\sqrt{p(\frac{\pi}{2} - z) p(\frac{\pi}{2} + z)}}. \quad (\text{S48})$$

Rescaling $z' = (E_J/E_C)^{1/4} z$ brings out a factor of $(E_C/E_J)^{1/4}$ in front of the integral, the integrand of which can now be seen to be Gaussian, peaked at $z = 0$. This Gaussian dominates in the asymptotic limit, such that we can treat it as a Gaussian integral in the range $-\infty < z < \infty$, with all other subleading contributions to the integrand evaluating at $z = 0$, i.e

$$\begin{aligned} &= \left(\frac{C_0 e^{\frac{1}{4}} \sqrt{\tan(\pi/8)}}{\sqrt{p(\frac{\pi}{2})}} \right)^2 \left(\frac{E_C}{2E_J} \right)^{-\frac{1}{4}} e^{-2\sqrt{\frac{2E_J}{E_C}} \left(1 - \frac{1}{\sqrt{2}} \right)} \left(\frac{E_C}{E_J} \right)^{1/4} \int_{-\infty}^{\infty} dz e^{-\frac{1}{4} z^2} \\ &= \left(\frac{C_0 e^{\frac{1}{4}} \sqrt{\tan(\pi/8)}}{\sqrt{p(\frac{\pi}{2})}} \right)^2 \left(\frac{E_C}{2E_J} \right)^{-\frac{1}{4}} e^{-2\sqrt{\frac{2E_J}{E_C}} \left(1 - \frac{1}{\sqrt{2}} \right)} \left(\frac{E_C}{E_J} \right)^{1/4} \sqrt{4\pi}. \end{aligned} \quad (\text{S49})$$

The constant $C_0 = \sqrt{(\pi e)^{-1/2} \sqrt{E_J/(2E_C)}}$ is worked out in [53]. Plugging this in,

$$\mathcal{O}_0 \equiv \int d\varphi \psi(\varphi) \psi(\pi - \varphi) = \frac{\tan(\pi/8)}{2^{-7/4}} e^{-(2-\sqrt{2})\sqrt{\frac{2E_J}{E_C}}}. \quad (\text{S50})$$

b. *Overlap of the gradient \mathcal{O}_1*

For clarity, let us rewrite Eqn S46 as $\psi(\varphi) = \frac{N}{\sqrt{p(\varphi)}} e^{-\frac{1}{3\sqrt{2}} \sqrt{\frac{2E_J}{E_C}} \left(-1 + \left(1 + \frac{\pi}{2} - \varphi \right)^{3/2} \right)} e^{-\frac{1}{\sqrt{2}} \left(1 - \sqrt{1 + \frac{\pi}{2} - \varphi} \right)}$, where all φ -independent terms have been coalesced into the prefactor N . As written, the φ -dependence of the wavefunction is a product of three parts, the most relevant of which is the first exponential carrying the argument scaled by $\sqrt{E_J/E_C}$. The overlap of the gradient

$$-\mathcal{O}_1 \equiv \int d\varphi \psi(\pi - \varphi) (-\partial_\varphi) \psi(\varphi) \quad (\text{S51})$$

is dominated by the derivative of this exponential, so long as it does not vanish (which we will see it does not). Thus

$$= \int d\varphi \psi(\pi - \varphi)\psi(\varphi)\partial_\varphi \left(\frac{1}{3\sqrt{2}} \sqrt{\frac{2E_J}{E_C}} \left(-1 + \left(1 + \frac{\pi}{2} - \varphi\right)^{3/2} \right) \right), \quad (\text{S52})$$

where we have dropped the sub-leading corrections. Continuing with the derivative,

$$= \frac{1}{2} \sqrt{\frac{E_J}{E_C}} \int d\varphi \psi(\pi - \varphi)\psi(\varphi) \sqrt{1 + \frac{\pi}{2} - \varphi}. \quad (\text{S53})$$

As demonstrated previously, the overlap $\psi(\varphi)\psi(\pi - \varphi)$ is dominated by the product of their dominate exponentials, which forms a strong Gaussian peak centered on $\varphi = \pi/2$. We then have

$$= \frac{1}{2} \sqrt{\frac{E_J}{E_C}} \int d\varphi \psi(\pi - \varphi)\psi(\varphi), \quad (\text{S54})$$

or equivalently

$$\mathcal{O}_1 = -\frac{1}{2} \sqrt{\frac{E_J}{E_C}} \mathcal{O}_0. \quad (\text{S55})$$